

Article

Effect of Saturation on Shear Behavior and Particle Breakage of Coral Sand

Xiang Chen ¹, Jianhua Shen ^{1,*}, Xing Wang ^{2,3} , Ting Yao ¹ and Dongsheng Xu ⁴ 

¹ State Key Laboratory of Geotechnical Mechanics and Engineering, Institute of Rock and Soil Mechanics, Chinese Academy of Sciences, Wuhan 430071, China

² School of Civil Engineering, Guangzhou University, Guangzhou 510006, China

³ Earthquake Engineering Research & Test Center, Guangzhou University, Guangzhou 510405, China

⁴ School of Civil Engineering and Architecture, Wuhan University of Technology, Wuhan 430062, China

* Correspondence: jhshen@whrsm.ac.cn

Abstract: Coral sand is the main filling material for the island–reef foundation. Under tidal actions, the saturation (S_r) of coral sand layers varies with the specific depths in the reclaimed foundation. Studying the S_r effect of coral sand’s mechanical behaviors is crucial for the stability of the reclaimed foundation of island–reefs. In this study, a “quantitative injection method” was designed to prepare coral sand with saturation ranging from 90% to 100%, and unconsolidated–undrained (UU) triaxial shear tests were conducted on coral sand under different effective confining pressures (σ'_3). The results indicated that the stress–strain curves of coral sand under various conditions were of the strain-softening type. When $\sigma'_3 = 200, 400, 600,$ and 800 kPa, the shear strength of coral sand decreased exponentially by 13.1, 9.1, 16.8, and 15.2%, respectively, with the increase in S_r from 90% to 100%. As S_r rose, the internal friction angle (φ) dropped by 3.77° . The cohesion (c) was not significantly affected by S_r compared to φ . In consideration of the physical susceptibility of coral sand to breakage, relative breakage ratio (B_r) and modified relative breakage index (B_r^*) were introduced to evaluate the particle breakage behaviors of coral sand samples with different S_r levels in the triaxial shear process. It was found that B_r and B_r^* increase linearly with increasing S_r ; the effect of S_r on the particle breakage of coral sand weakens significantly when σ'_3 is sufficiently large. The median particle size (d_{50}) of coral sand decreases with increasing S_r , and presents a negative linear correlation with both B_r and B_r^* . Based on comparing the strength and particle breakage characteristics of coral sand samples with varying S_r levels, this study suggests that 92.5% should be considered as the S_r value of coral sand available for testing.



Citation: Chen, X.; Shen, J.; Wang, X.; Yao, T.; Xu, D. Effect of Saturation on Shear Behavior and Particle Breakage of Coral Sand. *J. Mar. Sci. Eng.* **2022**, *10*, 1280. <https://doi.org/10.3390/jmse10091280>

Academic Editors:

Mohamed Benbouzid, Anne Blavette and Nicolas Guillou

Received: 29 July 2022

Accepted: 7 September 2022

Published: 10 September 2022

Publisher’s Note: MDPI stays neutral with regard to jurisdictional claims in published maps and institutional affiliations.



Copyright: © 2022 by the authors. Licensee MDPI, Basel, Switzerland. This article is an open access article distributed under the terms and conditions of the Creative Commons Attribution (CC BY) license (<https://creativecommons.org/licenses/by/4.0/>).

Keywords: coral sand; saturation; effective confining pressure; shear behavior; particle breakage

1. Introduction

Coral sand, also known as calcareous sand, is a geomaterial composed primarily of CaCO_3 [1,2]. Coral sand is mainly distributed on both sides of the equator in the Pacific Ocean, the Indian Ocean, the Atlantic Ocean, and the South China Sea [3]. In recent years, China has launched large-scale island–reef reclamation construction projects in the South China Sea [4]. According to its natural geographical advantages (i.e., island–reefs in the South China Sea are far from the mainland) and excellent engineering characteristics, coral sand has become the preferred material for island–reef foundation filling and infrastructure construction [5–7]. The reclaimed layers of island–reefs are only 3–5 m thick [8]. Under tidal actions, coral sand, as the filling material of bearing strata, is generally in a highly saturated (but not fully saturated) state [9]. Therefore, studying the effects of saturation (S_r) on the engineering mechanical properties of coral sand is crucial for the stability of the reclaimed foundation of island–reefs.

Triaxial shear tests can simulate the stress state of geomaterials in strata [10]. Therefore, predecessors mostly used triaxial shear tests to study the engineering mechanical properties

of coral sand and achieved some research results (Table 1) [11–18]. However, predecessors primarily utilized saturated coral sand as the research object but rarely touched upon the engineering mechanical properties of unsaturated coral sand [19]. Coral sand has a poor water-holding capacity [20], and it is difficult to precisely arrange coral sand samples with different S_r levels [21,22]. Water loss is also inevitable when filling coral sand with design S_r into the mold. These reasons may explain why predecessors have infrequently explored the engineering mechanical properties of unsaturated coral sand. Before investigating the engineering mechanical properties of coral sand samples with different S_r levels based on triaxial shear tests, the first critical technical problem to be solved is to develop a new sample preparation method. Next, if coral sand undergoes isotropic compression prior to triaxial shear tests, pore water will inevitably overflow from the sample, decreasing S_r . It will also be impossible to monitor the change in the S_r of coral sand during this process using conventional triaxial shear test apparatus. Therefore, it is preferable to investigate the engineering mechanical properties of coral sand samples with varying S_r using unconsolidated–undrained (UU) triaxial shear tests.

Table 1. Previous research on mechanical properties of coral sand based on triaxial shear test.

Research Material	Research Content	Research Method	Researcher and Year	Shear Type	Research Variable	Main Conclusions
Saturated coral sand	Mechanical properties	Triaxial shear test	Sharma and Ismail (2006) [11]	CU	Soil origin, Relative density, Initial mean effective stress	The monotonic shear response of calcareous soil from Goodwyn and Ledge Point was similar to that of siliceous sand, and the peak friction angle were relatively higher than siliceous sand.
			Hassanlourad et al. (2014) [12]	CU	Effective confining pressure, Relative density	Coral sand illustrated more shear strength than quartz sand in the triaxial consolidated undrained test.
			Zhang et al. (2019) [13]	CD	Fine particle content	The dilatancy property and peak deviator stress of coral sand decreased with the increasing fine particle content.
			Wu et al. (2020) [14]	CD	Effective confining pressure, Relative density	The strain softening and dilatation characteristic of coral sand gradually weaken with increasing effective confining pressure and decreasing compactness.
			Saeidaskari et al. (2021) [15]	CU	Effective confining pressure, Relative density	Coral sand showed initial contractive behavior, and the contractive behavior became more apparent as the effective confining pressure increased.
			Liu et al. (2022) [16]	CU	Effective confining pressure, Relative density	The shear modulus of coral sand increased with effective confining pressures and relative density, and the shear strength (or internal frictional angle) in peak state was more than that in critical state.
			Wang et al. (2022) [17]	CD	Particle size, Effective confining pressure	The shear strength of coral sand specimens with a single particle size decreased with an increase in particle size.
			Chen et al. (2022) [18]	CD	Particle gradation, Effective confining pressure	The softening and dilatancy were more significant for coral sand with smaller particle size, and the average peak friction angle of coral sand decreased linearly with the increasing mean particle size.

Moreover, coral sand is a special geomaterial susceptible to particle breakage even under low stress [23]. Predecessors also studied the particle breakage characteristics of coral sand, relying on triaxial shear tests (Table 2) [14,18,24–29]. They discovered how factors such as particle size, stress, and compactness affect the particle breakage of coral sand. However, the impact of S_r on the particle breakage of coral sand is seldom reported [30,31]. Indeed, the stress state significantly affects the particle breakage of coral sand [32,33]. It should be noted that the above findings are primarily obtained from consolidated-drained (CD) or consolidated-undrained (CU) triaxial shear tests and that the stress state of coral sand in UU triaxial shear tests differs greatly from CD or CU. Accordingly, the applicability of the above results to coral sand in UU triaxial shear tests must still be confirmed by solid test data, and related research should be expanded.

Table 2. Pervious research on particle breakage of coral sand based on triaxial shear test.

Research Material	Research Content	Research Method	Researcher and Year	Shear Type	Research Variable	Main Conclusions
Saturated coral sand	Particle breakage	Triaxial shear test	Zhang et al. (2008) [24]	CD	Effective confining pressure, Axial strain	The increase of effective confining pressure and axial strain could promote the particle breakage of coral sand.
			Shahnazari and Rezvani (2013) [25]	CD, CU	Effective confining pressure, Relative density, Axial strain, Drainage condition, Grain size distribution	Increasing of effective confining pressure, axial strain, relative density and grain size resulted in a higher particle breakage for coral sand, and coral sand under undrained condition had less particle breakage compared to the drained experiments due to the increasing of pore pressure.
			Yu (2018) [26]	CD, CU	Effective confining pressure, Initial void ratio, Consolidated stress ratio	In isotropic consolidation, more particle breakage of coral sand was caused in higher effective confining pressure (or denser sample), and anisotropic stress yielded more particle breakage than isotropic stress for coral sand.
			Wu et al. (2020) [14]	CD	Effective confining pressure, Relative density	The relationship between particle breakage and plastic work of coral sand could be described by a power function with a negative index, and particle breakage increased with the increasing plastic work with a hyperbolic form.
			Wang et al.(2021) [27]	CD, CU	Effective confining pressure, Axial strain	Particle breakage of coral sand increased with axial strain at a gradually decreasing rate during triaxial drained compression, and shear strain could induce further breakage without an increase in stress.
			Wang et al.(2021) [28]	CD	Effective confining pressure, Relative density	For coral gravelly sand, the highest breakage degree was observed in sand particles within 1–2 mm size range.
			Chen et al. (2022) [18]	CD	Particles gradation Effective confining pressure	The particle breakage of coral sand increased with the increasing effective confining pressure and mean particle size.
			Shen et al. (2022) [29]	CU	Effective confining pressure	The particle breakage of coral sand increased in powder function form with increasing effective confining pressure, and splitting and abrasion were the main particle breakage patterns of coral sand within 400 kPa effective confining pressure.

In light of this, an independently designed “quantitative injection method” was used in this study to prepare coral sand samples with various S_r levels. The UU triaxial shear tests were conducted on these samples under different effective confining pressures (σ'_3) to ascertain the S_r effect of the coral sand shear behavior. Finally, screening tests were performed on tested samples to understand the particle breakage behaviors of coral sand samples with different S_r levels during UU triaxial shear tests. The study’s results provide theoretical support for assessing the stability of the reclaimed foundation of island–reefs.

2. Test Overview

2.1. Material

This study uses uncemented loose coral sand collected from a hydraulically reclaimed island–reef in the South China Sea. Figure 1 exhibits the uniform initial gradation of coral sand with particle sizes ranging from 0.25 to 0.5 mm. Its nonuniformity coefficient (C_u) and curvature coefficient (C_c) are 1.455 and 0.96, respectively (Table 3). According to the *Chinese National Standard of Soil Test Method* (GB/T 50123–2019), it should be named as poorly graded coral medium sand. The specific gravity (G_s), maximum dry density (ρ_{dmax}), and minimum dry density (ρ_{dmin}) of coral sand are 2.83, 1.385, and 1.085, respectively. According to GB/T 50123–2019, the minimum void ratio (e_{min}) and maximum void ratio (e_{max}) of calcareous sand are 1.043 and 1.608, respectively.

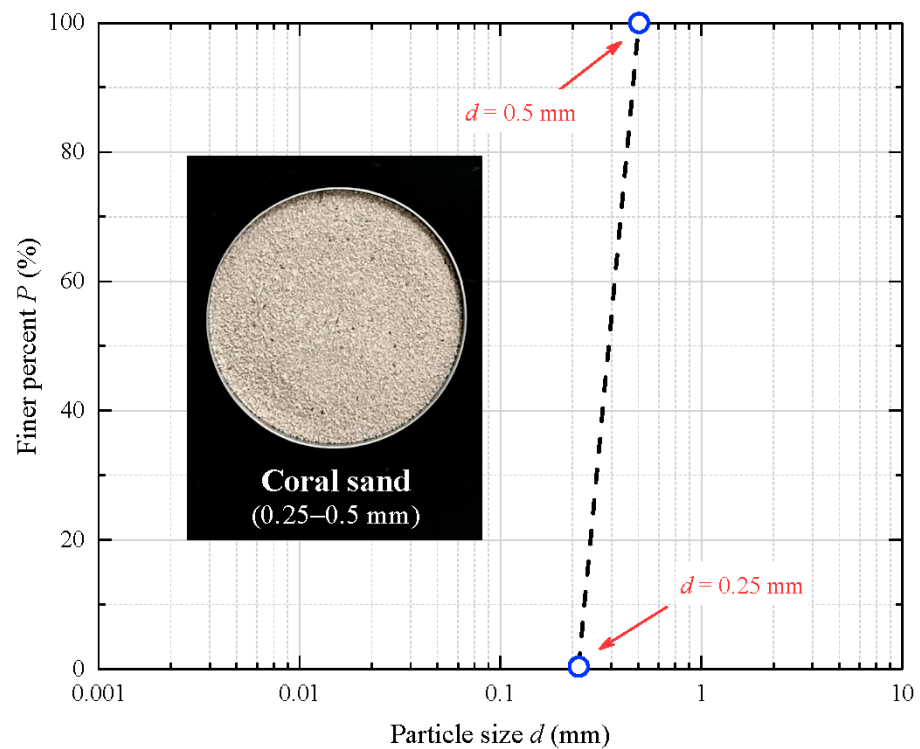


Figure 1. Particle distribution curve of coral sand.

Table 3. Physical parameters of coral sand.

Sample	Particle Size d (mm)	Median Size d_{50} (mm)	Nonuniform Coefficient C_u	Curvature Coefficient C_c	Specific Gravity G_s	Maximum Void Ratio e_{max}	Minimum Void Ratio e_{min}	Maximum Dry Density ρ_{dmax} (g/cm ³)	Minimum Dry Density ρ_{dmin} (g/cm ³)
Coral medium sand	0.25–0.5	0.375	1.455	0.96	2.83	1.608	1.043	1.385	1.085

2.2. Test Scheme

This study analyzes the effects of S_r on the shear behavior and particle breakage behavior of coral sand using UU triaxial shear tests. The selection of S_r was determined by considering the following two assumptions: (I) All the pores in coral sand are in a closed state, and the effect of the inner pores released due to particle breakage in the shear process on test results can be ignored; (II) the S_r of coral sand is 100% when interparticle pores are filled up with water. Considering these assumptions and the nearly saturated state of coral sand in most reclaimed layers, the S_r of coral sand was set at 100, 97.5, 95, 92.5,

and 90% utilizing a gradient of 2.5%, respectively. The S_r effect of the shear behavior of coral sand was studied using UU triaxial shear tests to avoid the change in the S_r of coral sand caused by water loss during consolidation and shear processes. After foundation treatment, coral sand can generally reach a compact state [28]. Hence, coral sand in shear tests was set with a relative density (D_r) of 70% to simulate its actual physical state in strata as realistically as possible. The σ'_3 applied to coral sand was 200, 400, 600, and 800 kPa. These σ'_3 settings covered multiple environments from low to high stress and were intended to investigate the S_r effect of the shear behavior of coral sand over a broad stress range. All coral sand samples were $\text{Ø}39.1 \times 80$ mm in size (diameter \times height). Shearing proceeded at a 0.15 mm/min rate and stopped when axial strain (ϵ_a) reached 30% (Table 4). It is noteworthy that coral sand is a geomaterial highly susceptible to breakage [34]. Screening tests were performed on samples to assess the particle breakage behaviors of coral sand samples with different S_r levels during the UU triaxial shear process.

Table 4. Triaxial shear test scheme.

Sample	Sample No.	Saturation S_r (%)	Relative Density D_r (%)	Specimen Size		Effective Confining Pressure σ'_3 (kPa)	Shear Type	Shear Rate v (mm/min)	Terminal Strain ϵ_t (%)
				Diameter (mm)	Height (mm)				
Coral medium sand	CS-90	90	70	39.1	80	200	UU	0.15	30
	CS-90	90	70	39.1	80	400	UU	0.15	30
	CS-90	90	70	39.1	80	600	UU	0.15	30
	CS-90	90	70	39.1	80	800	UU	0.15	30
	CS-92.5	92.5	70	39.1	80	200	UU	0.15	30
	CS-92.5	92.5	70	39.1	80	400	UU	0.15	30
	CS-92.5	92.5	70	39.1	80	600	UU	0.15	30
	CS-92.5	92.5	70	39.1	80	800	UU	0.15	30
	CS-95	95	70	39.1	80	200	UU	0.15	30
	CS-95	95	70	39.1	80	400	UU	0.15	30
	CS-95	95	70	39.1	80	600	UU	0.15	30
	CS-95	95	70	39.1	80	800	UU	0.15	30
	CS-97.5	97.5	70	39.1	80	200	UU	0.15	30
	CS-97.5	97.5	70	39.1	80	400	UU	0.15	30
	CS-97.5	97.5	70	39.1	80	600	UU	0.15	30
	CS-97.5	97.5	70	39.1	80	800	UU	0.15	30
	CS-100	100	70	39.1	80	200	UU	0.15	30
	CS-100	100	70	39.1	80	400	UU	0.15	30
	CS-100	100	70	39.1	80	600	UU	0.15	30
	CS-100	100	70	39.1	80	800	UU	0.15	30

2.3. Apparatus and Procedure

The test apparatus is a TKA-Advanced full-automatic stress path triaxial testing apparatus manufactured by Nanjing TKA Technology Co., Ltd. (Nanjing, China) (Figure 2). It mainly consists of a pressure chamber, a displacement sensor, a load sensor, a data acquisition system, a strain control system, and pressure/volume controllers (used to control confining and back pressure). The apparatus supports variable-speed loading and has a shear rate range of 0.0001–9.9999 mm/min. The load sensor has a range of 10 kN and a precision of 0.15% F.S. The two pressure/volume controllers have a stress control range of 0–2000 kPa (precision = 1 kPa), and a volume range of 250 mL (precision = 0.001 mL). The LCD screen on each pressure/volume controller displays the current confining pressure/back pressure and the volume of water inside. The on-screen keyboard can be employed to regulate stress and absorb or drain water by the specified volume.

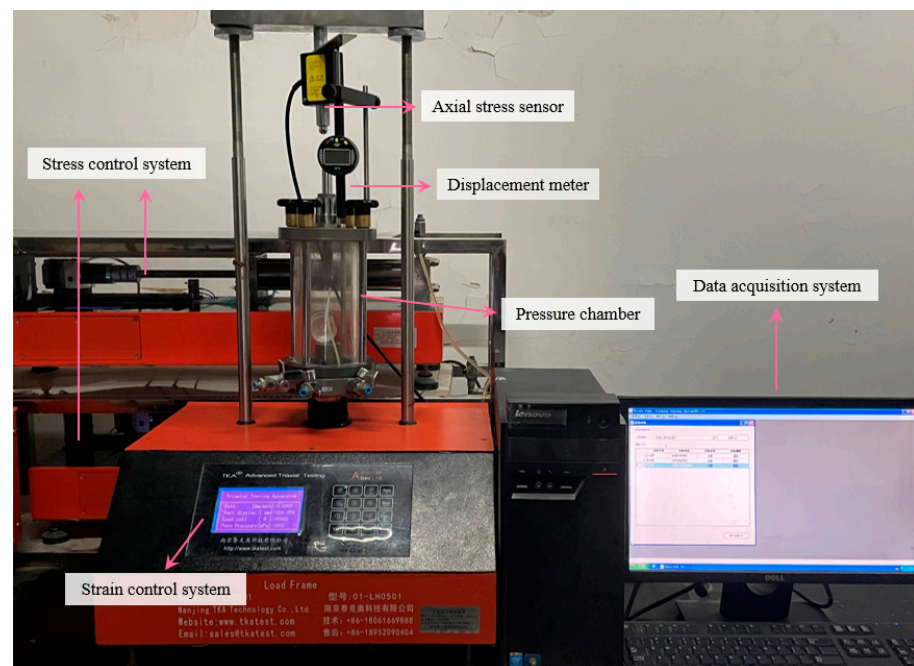


Figure 2. Full-automatic stress path triaxial apparatus.

Precise control of S_r is the most critical step in studying the S_r effect on the shear behavior of coral sand. Most predecessors control the water content of a sample by first preparing a sample with designed water content and then transferring the sample into a rubber membrane [35–37]. This approach is ideal for regulating the water content of fine-grained soils (such as clay and silt). Due to the poor water-holding capacity of coral sand, it is difficult to prevent water overflow when loading a sample of coral sand with designed water content into the rubber membrane. Therefore, an original method was designed to prepare coral sand samples with different S_r levels as follows.

(1) The dry density of the sample under 70% D_r was determined utilizing the physical parameters listed in Table 1. The mass of the dry sample was calculated from dry density and sample size, and dry coral sand was weighed accordingly (Figure 3a). An impermeable stone was placed on the base of the pressure chamber, sheathed by the rubber membrane, and fixed using a split mold. A vacuum pump was connected to the interface outside of the split mold to remove the gas between the rubber membrane and the split mold's inner wall, allowing the rubber membrane to perfectly fit with the split mold's inner wall (Figure 3b).

(2) The sample was loaded into the rubber membrane by five layers through sand alluviation. Each time a layer was loaded, a graduated scale was used to measure the distance between the sample surface and the split mold top to ensure the compactness of the sample matched that in Table 2 (Figure 3c). The sample surface was roughened before the next layer was added. The above steps were repeated until the sample's upper surface reached the same level as the top of the split mold. The sample cap was covered after the completion of sample loading. At this point, the preparation of a dry coral sand sample with 70% D_r was completed.

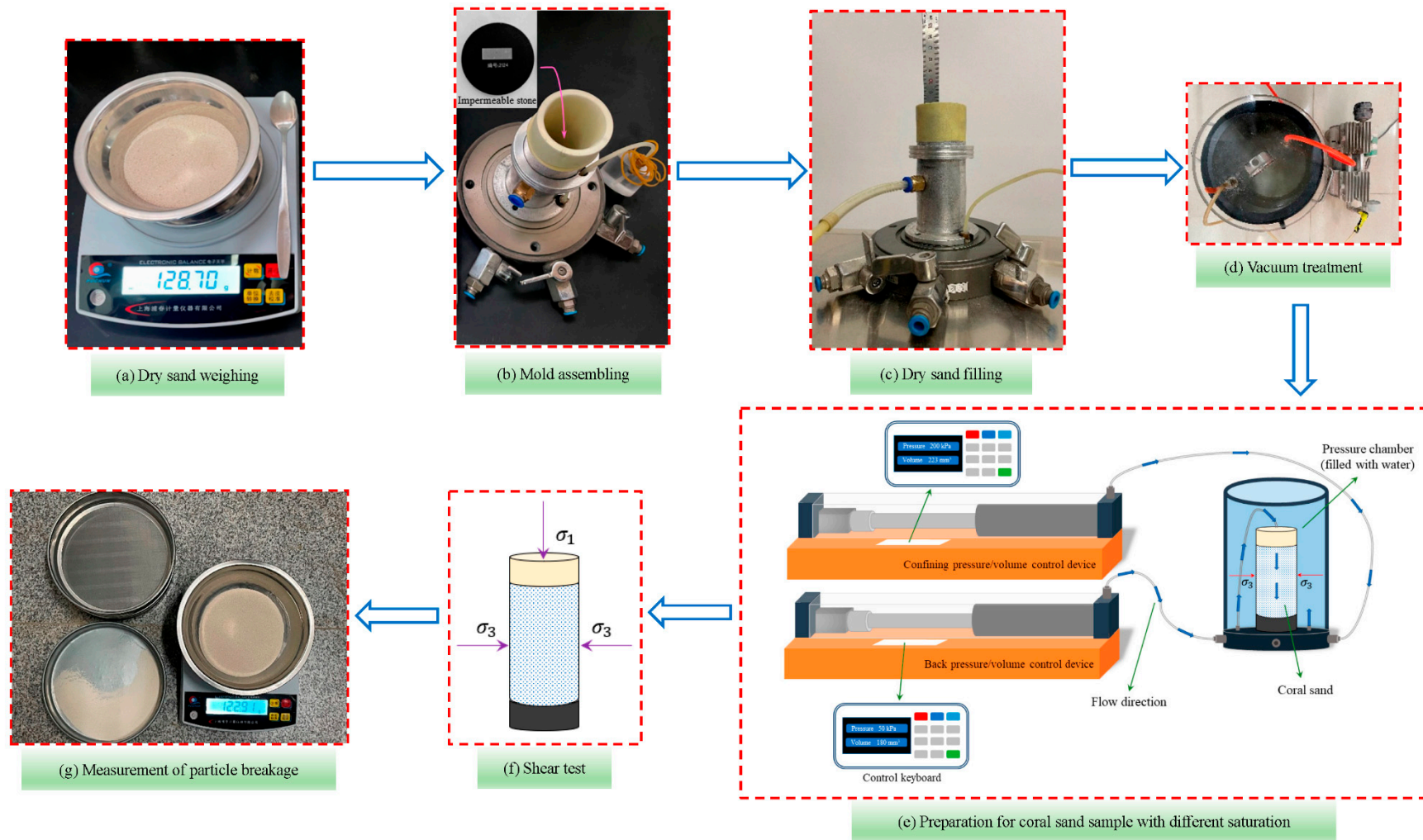


Figure 3. Diagrammatic sketch of test procedures.

(3) The theoretical water contents of coral sand samples with different S_r levels were calculated from the physical parameters and test parameters indicated in Tables 1 and 2 as follows:

$$Dr = \frac{e_{max} - e}{e_{max} - e_{min}} \tag{1}$$

$$n = \frac{e}{e + 1} \tag{2}$$

where n is porosity. The void ratio e of the coral sand sample with 70% Dr was calculated by Equation (1) and then substituted into Equation (2) to determine porosity n . The volume of water in the sample was computed as follows:

$$V_W = S_r \cdot V_V = S_r(n \cdot V) \tag{3}$$

where V_W is the volume of water in the sample, V_V is the volume of pores in the sample, and V is the total volume of the sample. The water contents of coral sand samples with different S_r levels were calculated by Equation (3) (Table 5). First, the sample was vacuum-treated to remove the gas inside (Figure 3d) and produce a negative pressure (to increase the seepage rate of water in the sample in the subsequent water injection process). Next, the pressure chamber was placed on the base of the triaxial shear apparatus, and water was injected into the pressure chamber so that the sample cap would come into contact with the load sensor. The confining pressure in the pressure chamber was set at 200 kPa. Multiple trial tests confirmed that a confining pressure of 200 kPa can prevent the volume expansion caused by increasing back pressure during the water injection process. After the confining pressure stabilized, the back pressure valve at the base of the pressure chamber was opened. The back pressure/volume controller was utilized to inject water into the sample until the corresponding S_r was achieved (Figure 3e). Due to the gradual filling of pores by water, back pressure will develop in the sample at this time. Finally, after the water injection was completed, the sample was left to rest for two hours, after which the back pressure value displayed on the back pressure/volume controller was recorded (denoted as x kPa). This value represents the back pressure value prior to shearing. The effective confining pressure was denoted as y kPa, in which case the actual confining pressure will be $(x + y)$ kPa.

Table 5. Water content of coral sand sample with different saturations.

Sample	Sample No.	S_r (%)	Water Content (mL)
Coral medium sand	CS-90	90	45.56
	CS-92.5	92.5	46.82
	CS-95	95	48.09
	CS-97.5	97.5	49.35
	CS-100	100	50.62

(4) UU triaxial shear tests were conducted on coral sand samples under design σ'_3 . Shearing was performed at a 0.15 mm/min rate and stopped when $\epsilon_a = 30\%$ (Figure 3f).

(5) After shear tests, samples were washed with clean water into the tray, which was placed in an oven with a constant temperature of 105 °C. It was removed after 24 h and allowed to cool down to room temperature. Then, screening tests were conducted on the samples to examine their particle gradation curves (Figure 3g). An excessively short screening time causes inadequate screening while an excessively long one aggravates particle breakage. As a result, the screening time was set at 15 min each time [24].

3. Shear Test Result and Analysis

3.1. Deviator Stress–Pore Water Stress–Axial Strain Relationship

Figure 4 shows the deviator stress–axial strain curves (i.e., $q-\epsilon_a$ curves) of coral sand samples under different conditions. It can be seen from Figure 4 that, within the σ'_3 range of

800 kPa, the $q-\varepsilon_a$ curves of coral sand samples with 90–100% S_r during the UU triaxial shear stress state presented a strain softening trend. The $q-\varepsilon_a$ curve of each coral sand sample can be divided into three stages:

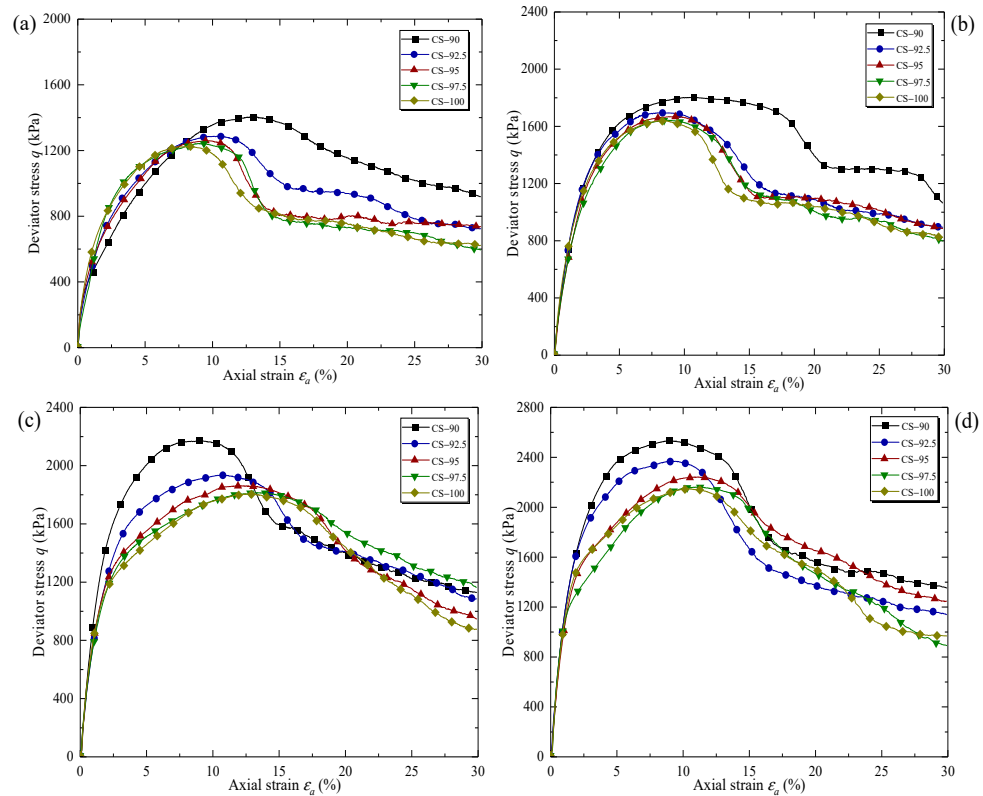


Figure 4. Deviator stress-axial strain curves of coral sand with different saturations: (a) $\sigma'_3 = 200$ kPa; (b) $\sigma'_3 = 400$ kPa; (c) $\sigma'_3 = 600$ kPa; (d) $\sigma'_3 = 800$ kPa.

(1) Elastic stage: In the initial shear stage, q surged with increasing ε_a , and the $q-\varepsilon_a$ curve was almost linear.

(2) Plastic yield stage: During the intermediate shear stage, q continued to grow with increasing ε_a , but at a gradually slower rate, and the $q-\varepsilon_a$ curve presented a gentle changing trend.

(3) Failure stage: In the late shear stage, due to increasing ε_a , q first peaked and then continued to decrease until the test was complete. The sample showed evident strain softening characteristics.

Figure 5 depicts the pore water stress-axial strain curves (i.e., $u-\varepsilon_a$ curves) of coral sand samples under different conditions. When $\sigma'_3 = 200$ kPa, u was negative, and the sample exhibited a dilatancy similar to dense sand [38]. When $\sigma'_3 = 400$ kPa, only CS-100 showed obvious dilation. When $\sigma'_3 = 600$ and 800 kPa, u was not negative, and the sample was always in a state of contraction. First, increasing σ'_3 tightened the constraint on the sample and prevented its dilation deformation [39]. Second, increasing σ'_3 aggravated the particle breakage of the sample in the shear process and reduced its dilation degree [40]. Therefore, when $\sigma'_3 = 600$ and 800 kPa, the sample remained in a state of contraction throughout the shear process.

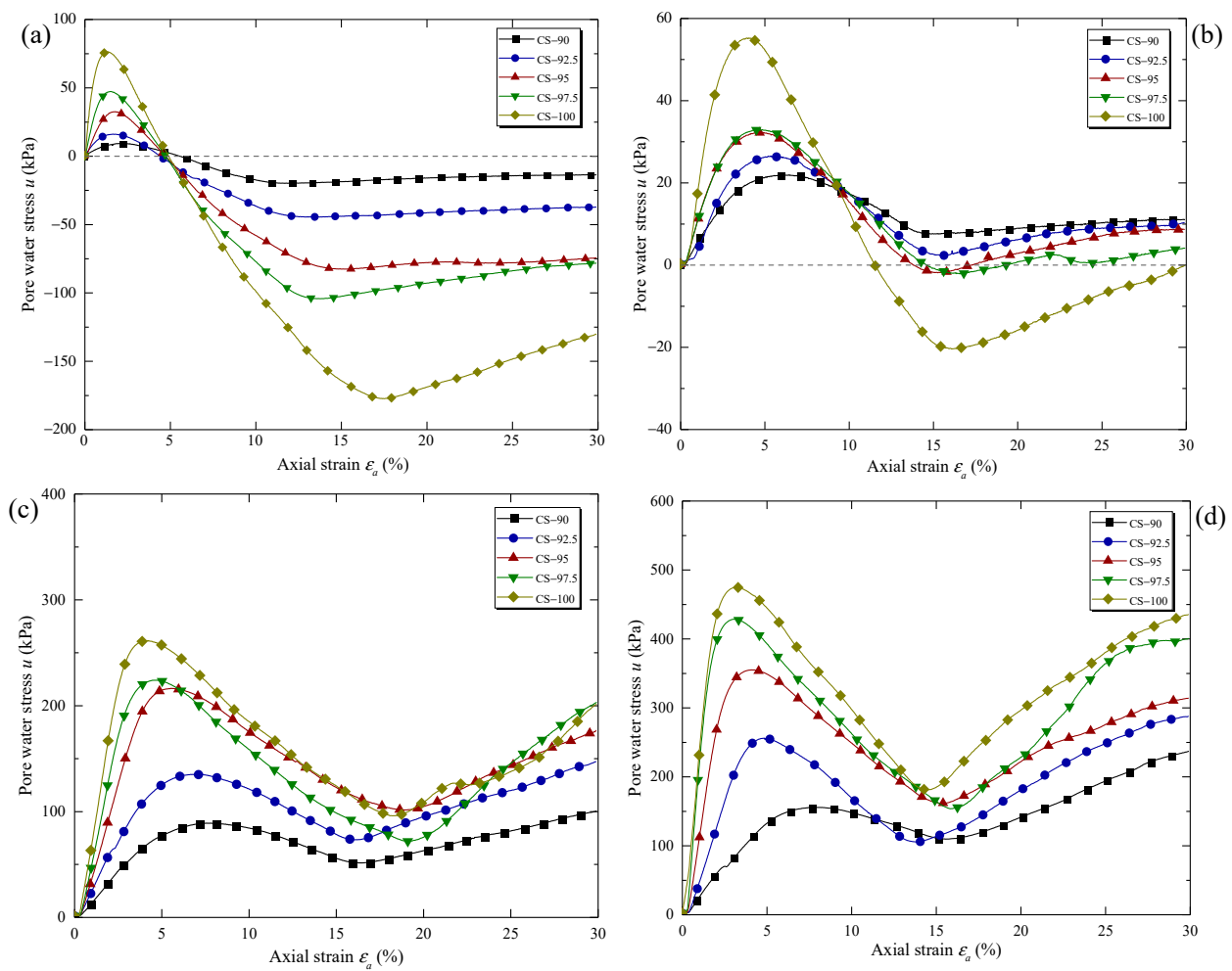


Figure 5. Pore water stress-axial strain curves of coral sand with different saturations: (a) $\sigma'_3 = 200$ kPa; (b) $\sigma'_3 = 400$ kPa; (c) $\sigma'_3 = 600$ kPa; (d) $\sigma'_3 = 800$ kPa.

Within the σ'_3 range of 800 kPa, $u-\varepsilon_a$ curves of coral sand samples with 90–100% S_r during the UU triaxial shear stress state can also be separated into three stages:

(1) In the initial shear stage, u rose rapidly with increasing ε_a , and the sample contracted. In the initial UU triaxial shear stage, the sample's pore water produced u under external loads. Growing ε_a (or shear stress τ) increased the mean effective stress (p') borne by the sample, resulting in sample contraction. Sample contraction also enhanced the squeezing action on pore water and caused u to present a growing trend with rising ε_a [41]. The peak pore water stress (u_{p1}) can be utilized to characterize the maximum contraction degree of coral sand samples. The curve of u_{p1} changing with S_r was plotted to explore the effect of S_r on u of a coral sand sample in the initial shear stage (Figure 6). According to Figure 6: (I) there is an apparent positive correlation between u_{p1} and S_r under the same σ'_3 . A sample with a higher S_r level contains more pore water content and also produces a more significant u under the constraint of σ'_3 . A positive correlation between u_{p1} and S_r indicates that a sample with a higher S_r level has a greater contraction degree in the initial shear stage. (II) For coral sand samples with the same S_r , u_{p1} increases more significantly under high effective confining pressures ($\sigma'_3 = 600$ and 800 kPa) than under low effective confining pressures ($\sigma'_3 \leq 400$ kPa), and the increments also increase with increasing S_r . This phenomenon was mainly caused by the constraint imposed by σ'_3 on coral sand samples. Under a low effective confining pressure ($\sigma'_3 \leq 400$ kPa), the constraining force was weak, and u was low and insensitive to the change in S_r . Increasing σ'_3 enhanced the constraining force, caused the increase of u , and amplified the effect of S_r on u .

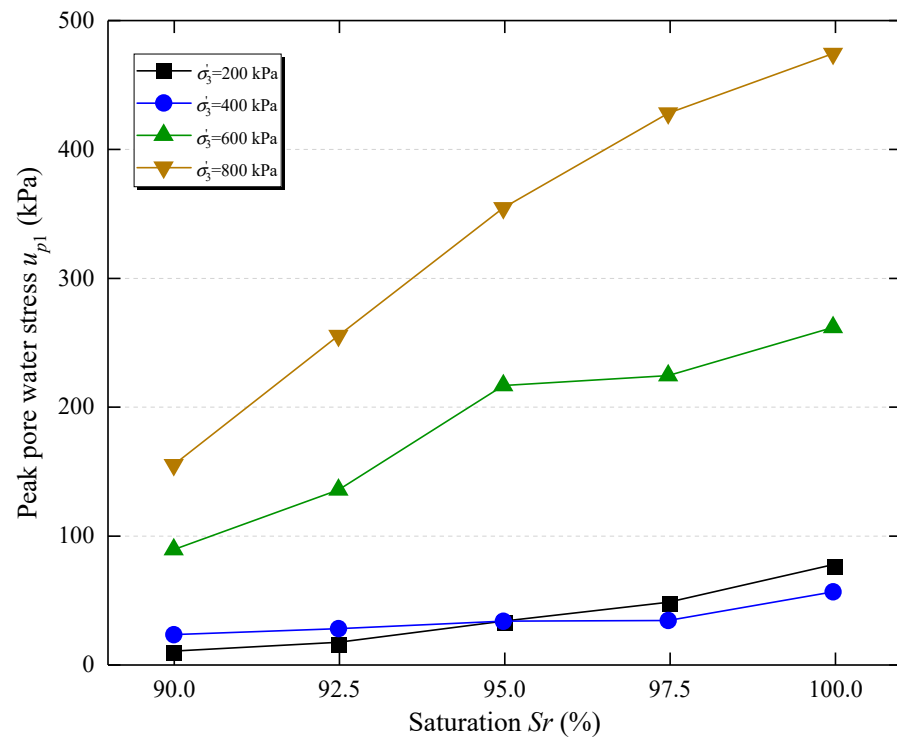


Figure 6. Relationship between peak pore water stress and saturation of coral sand.

(2) u gradually decreased with increasing ϵ_a after reaching u_{p1} . This was primarily due to the expansion of coral sand particles in the shear process. During the dilation process, coral sand particles bore more external loads. Moreover, the external loads carried by coral sand particles increased with increasing dilation degree, resulting in a decreasing trend for u .

(3) u increased with increasing ϵ_a after reaching the minimum (at which point coral sand particles had the largest dilation degree). The failure modes of coral sand samples with various S_r levels were essentially identical. Due to space limitations, Figure 7 only shows the post-test forms of coral sand samples with different S_r levels when $\sigma_3' = 200$ kPa. In the late shear stage, a shear band emerged gradually in coral sand samples (that is, local shear occurred) and slowly expanded with increasing ϵ_a . This was the fundamental reason why u increased with increasing ϵ_a after reaching the minimum.

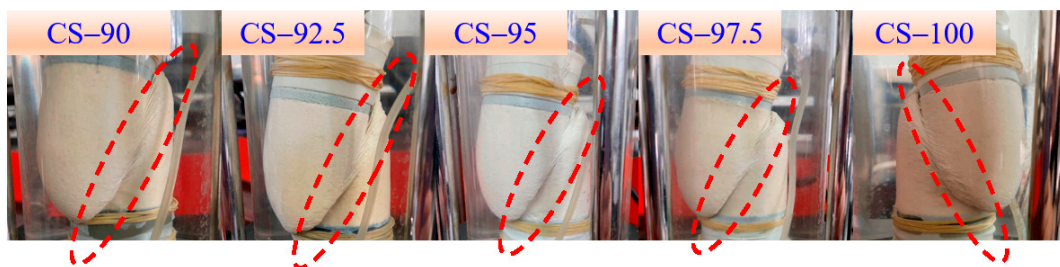


Figure 7. Failure pattern of coral sand samples after shear test.

3.2. Stress Path

Stress path curves are curves that describe the process of q' changing with p' in the triaxial shear process. In UU triaxial shear stress state, the q' and p' of a geomaterial can be expressed as:

$$q' = \sigma'_1 - \sigma'_3 \tag{4}$$

$$p' = \frac{\sigma'_1 + 2\sigma'_3}{3} \tag{5}$$

where σ'_1 and σ'_3 are effective major and minor principal stresses, respectively. When u reached the minimum, the sample experienced local shear (or the development of sample deformation was no longer homogeneous), so this study only discussed the stress paths of coral sand samples before u reached the minimum (Figure 8). As seen in Figure 8, coral sand samples with different Sr levels have similar stress paths under a low effective confining pressure ($\sigma'_3 \leq 400$ kPa). In the UU triaxial shear process, the difference in u was the macroscopic mechanism for which coral sand samples with various Sr levels showed different stress responses under the same σ'_3 . However, the change in Sr did not significantly affect the development of stress in coral sand samples, mainly because u was significantly lower than principal stresses (or there was no noticeable difference in u between coral sand samples with different Sr levels) under a low σ'_3 . For example, when $\sigma'_3 = 200$ kPa, the maximum deviation in u_{p1} between coral sand samples with different Sr levels was only 67.2 kPa. For this reason, the stress path curves of coral sand samples with different Sr levels showed no discernible differences from each other. When σ'_3 increased to 600 kPa (or 800 kPa), the maximum deviation in u_{p1} between coral sand samples with different Sr levels reached 173 kPa (or 320.1 kPa). As a result, the stress path curves of coral sand samples with many Sr levels differed significantly from each other under high effective confining pressures ($\sigma'_3 = 600$ and 800 kPa).

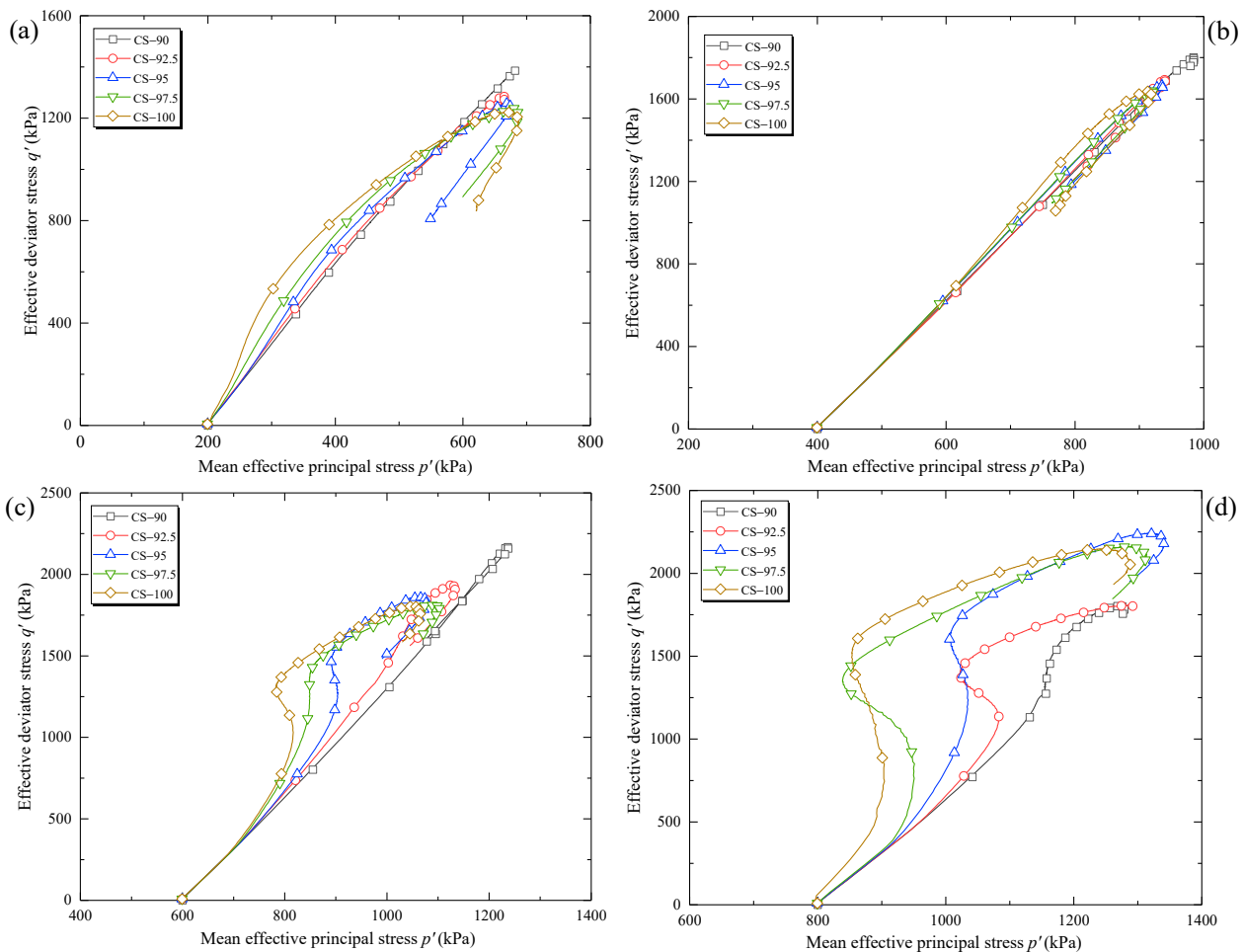


Figure 8. Stress path of coral sand with different saturations: (a) $\sigma'_3 = 200$ kPa; (b) $\sigma'_3 = 400$ kPa; (c) $\sigma'_3 = 600$ kPa; (d) $\sigma'_3 = 800$ kPa.

3.3. Initial Elastic Modulus

Initial elastic modulus (E_i) is an important indicator characterizing the stiffness of geomaterials, defined as the ratio of q to ε_a of the sample within the elastic limit [14]:

$$E_i = \frac{q}{\varepsilon_a} \tag{6}$$

Plastic deformation plays a dominant role in the deformation of coral sand under loads, while elastic deformation is minimal [42]. For this reason, the data within the range of $\varepsilon_a = 1\%$ were adopted to calculate E_i . Figure 9 shows the E_i of coral sand with S_r change under different conditions. As seen from Figure 9, E_i fluctuates within an extremely small range with changing S_r under the same σ_3' . E_i' was defined as the mean E_i of coral sand samples with different S_r levels under a certain σ_3' :

$$E_i' = \frac{E_{i1} + E_{i2} + \dots + E_{in}}{n} \tag{7}$$

where n is a natural constant, set at 1, 2, 3, and 4, respectively. With increasing σ_3' , E_i' gradually increased from 480.1 kPa to 1046.3 kPa (Figure 9). When σ_3' rose, the constraining force applied to the sample increased, and so did the slope of the $q-\varepsilon_a$ curve in the initial shear stage, as manifested by a positive correlation between E_i' and σ_3' . The results in Figure 9 also indicated that, compared to S_r , σ_3' exerted a more significant effect on the E_i of coral sand. In UU triaxial shear stress state, q grew much faster than u in the initial shear stage (Figures 4 and 5). Coral sand particles bore most external loads and experienced elastic deformation. Thus, S_r had no obvious effect on E_i .

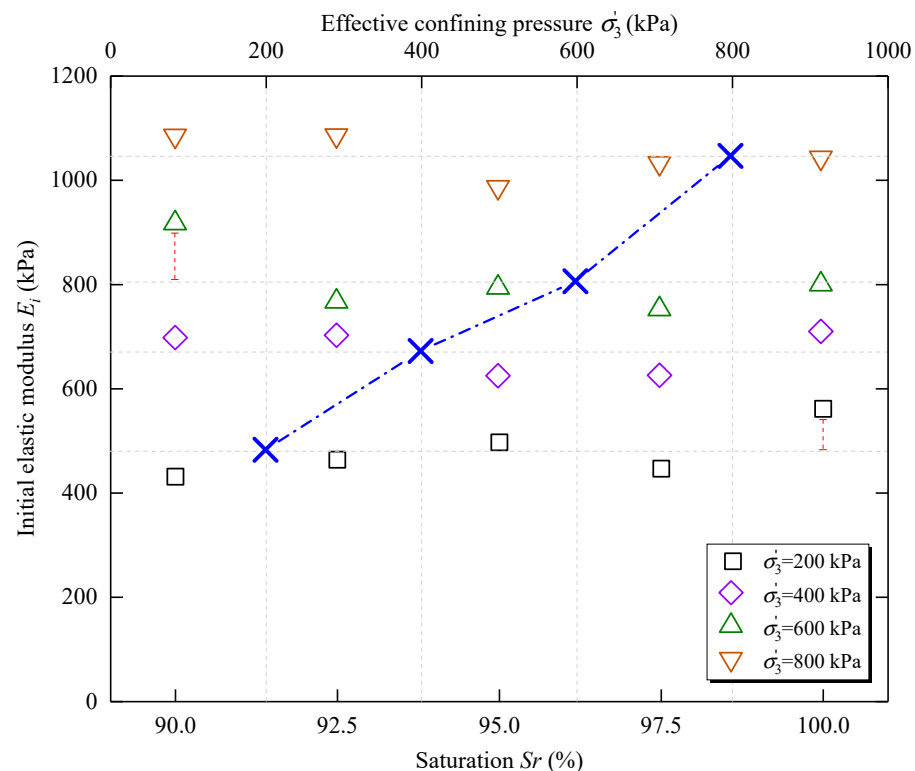


Figure 9. Relationship among initial elastic modulus, effective confining pressure and saturation of coral sand.

3.4. Shear Strength

Shear strength is an important indicator for characterizing the geomaterials' mechanical properties and a major parameter in geotechnical design [43,44]. The shear strength of a geomaterial depends on its type, meso-fabric, water content, and other factors [45–48].

Wiebe [49], Hu et al. [50], Malizia and Shakoor [51] studied terrigenous geomaterials and found that the soil shear strength decreased as water content increased. Due to its particular structure, coral sand contains numerous interparticle pores during the natural accumulation process [52], which can accommodate abundant water. Since sand particles and pore water share external loads, S_r will affect the shear strength of coral sand. In this section, peak deviator stress (q_p) was adopted to analyze the S_r effect of the shear strength of coral sand (Figure 10). Figure 10 indicates that the q_p of coral sand decreases with increasing S_r . For example, when $\sigma'_3 = 200$ kPa, the q_p of coral sand drops by 184.2 kPa with increasing S_r from 90% to 100%. When $\sigma'_3 = 600$ kPa, the q_p of coral sand decreases by 363.4 kPa as the S_r rises from 90% to 100%. Pore water can be divided into free, bound, and capillary water, among which free water drifts through interparticle pores and has good fluidity. Nearly saturated coral sand has the highest content of free water [9]. Free water weakens the frictional resistance between coral sand particles [53], which is an important part of the strength of coral sand. The content of free water grows as S_r raises, for which the strength of coral sand declines with increasing S_r .

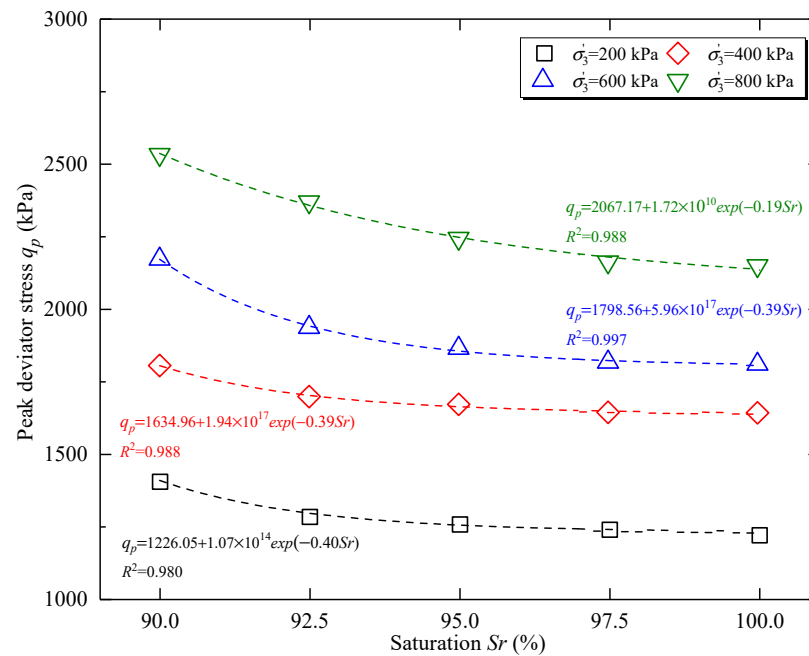


Figure 10. Relationship between peak deviator stress and saturation of coral sand.

Further analysis in this study found that the relationship between q_p and S_r could be expressed as:

$$q_p = m_1 + m_2 \exp(m_3 S_r) \tag{8}$$

where m_1 , m_2 , and m_3 are fitting parameters (Table 6). m_1 is approximately equal to the q_p of CS-100 under different σ'_3 levels. m_1 can characterize the shear strength of coral sand with 100% S_r , which is mainly affected by σ'_3 . m_2 and m_3 jointly control the amplitude by which the shear strength of coral sand increases with decreasing S_r . m_3 is a negative value that characterizes the negative correlation between shear strength and S_r . Measurement of unsaturated shear strength at an engineering site is complex and costly. Equation (8) can be applied to predict the shear strength of unsaturated coral sand.

Figure 11 shows how the difference in q_p between unsaturated coral sand and saturated coral sand changed with S_r , as seen in Figure 11.

Table 6. Peak deviator stress–saturation fitting expression and parameters.

Sample	Expression	σ'_3 (kPa)	m_1	m_2	m_3	R^2
Coral medium sand	$q_p = m_1 + m_2 \exp(m_3 S_r)$	200	1226.055	1.068×10^{18}	-0.404	0.980
		400	1634.959	1.939×10^{17}	-0.385	0.988
		600	1798.559	5.955×10^{17}	-0.389	0.997
		800	2067.165	1.717×10^{10}	-0.194	0.988

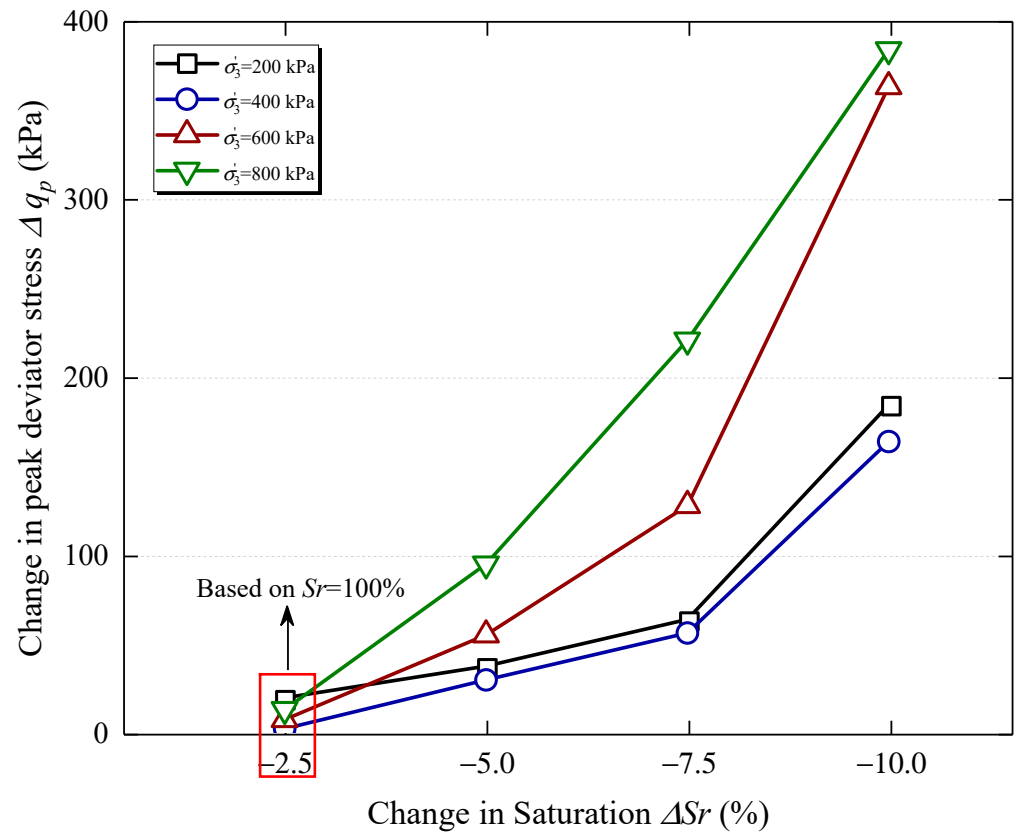


Figure 11. Variations in the peak deviatoric stress with saturation of coral sand.

(1) Under the same σ'_3 , the difference in q_p between unsaturated and saturated coral sand increased with increasing S_r . This law was represented in Figure 11 as the gradual increase in the slope of the linear segment, which coincided with the law expressed by Equation (8) (that is, the decreasing trend of q_p with increasing S_r was gradually weakened). It was because increasing S_r weakened the shear strength of coral sand.

(2) Clearly, increasing σ'_3 grew the difference in q_p between unsaturated and saturated coral sand. The S_r effect of the shear strength of coral sand was significantly affected by σ'_3 . For example, under a low effective confining pressure ($\sigma'_3 \leq 400$ kPa), when S_r decreased from 97.5% to 92.5%, the maximum difference in q_p between unsaturated and saturated coral sand was 63.4 kPa only. In contrast, under high effective confining pressures ($\sigma'_3 = 600$ and 800 kPa), when S_r decreased from 97.5% to 92.5%, the maximum differences in q_p between unsaturated and saturated coral sand were 127.6 kPa and 220.8 kPa, respectively. Under a low effective confining pressure ($\sigma'_3 \leq 400$ kPa), u in a coral sand sample can be disregarded in relation to its axial stress. However, increasing σ'_3 caused u to increase significantly, for which the ratio of u to axial stress also increased obviously. In other words, σ'_3 affected the shear strength of a coral sand sample by affecting u in the sample. For this reason, the shear strength of coral sand samples with different S_r levels uniformly showed an obvious confining pressure effect.

3.5. Shear Strength Parameter

According to the Mohr–Coulomb strength theory, the strength of a geomaterial mainly consists of two parts, frictional and cohesive strength:

$$\tau = c + \sigma \tan \varphi \tag{9}$$

where σ is the normal stress applied on the shear plane, φ is the internal friction angle, c is cohesion. The Mohr’s stress circles and shear strength envelope curves of coral sand samples with different S_r levels can be depicted using Equation (9) and test results (Figure 12). As shown in Figure 12, for coral sand samples with the same S_r , their shear strength envelope curves are tangent to Mohr’s stress circles under different σ'_3 levels. The slopes of shear strength envelope curves and the intercepts with the τ axis can be utilized to determine the shear strength parameters of coral sand samples with different S_r levels.

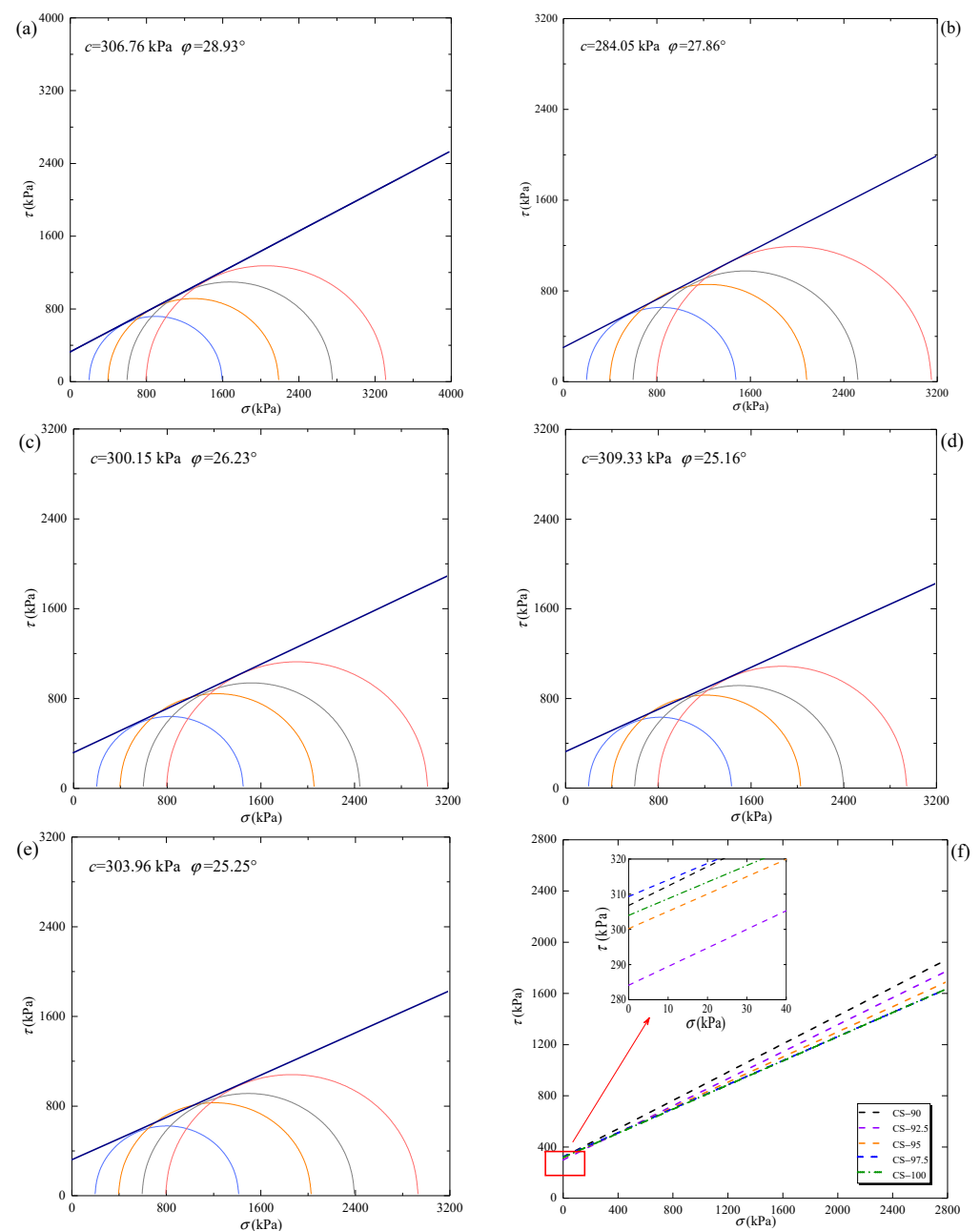


Figure 12. The shear strength envelope curves of: (a) CS-90; (b) CS-92.5; (c) CS-95; (d) CS-97.5; (e) CS-100; and (f) the comparison.

Figure 13 shows the relationships of the shear strength parameters of coral sand with S_r . According to the results in Figure 13.

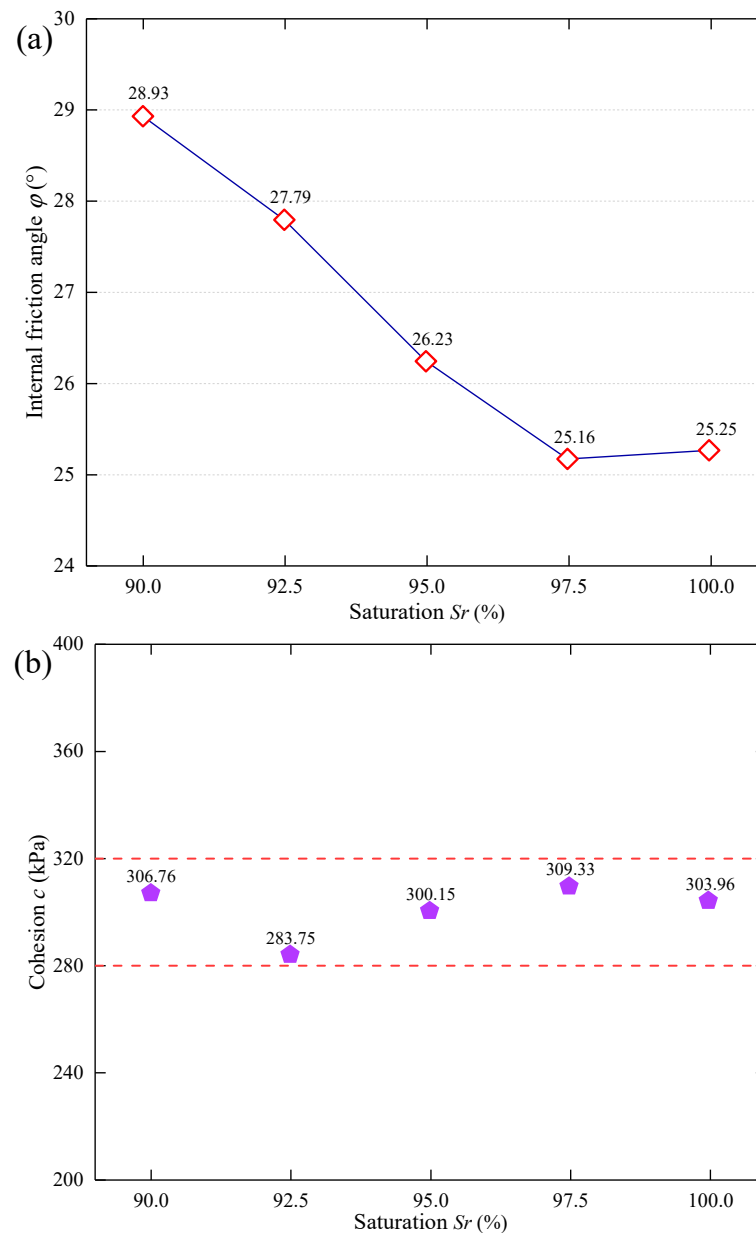


Figure 13. Relationship between strength parameter and saturation of coral sand: (a) internal friction angle; (b) cohesion.

(1) Within the σ'_3 range of 800 kPa, the ϕ values of coral sand samples with 90–100% S_r in UU triaxial shear stress state fell within the range of 25–29° (Figure 13a). When S_r increased successively from 90% to 97.5%, the ϕ of coral sand decreased approximately linearly by 3.77°. When S_r increased from 97.5% to 100%, ϕ remained almost unchanged. Classical soil mechanics holds that the ϕ of geomaterials can be expressed as [54,55]:

$$\phi = \phi_u + \phi_d + \phi_b \tag{10}$$

where ϕ_u is sliding friction angle, ϕ_d is the friction angle caused by dilation, ϕ_b is the friction angle caused by particle breakage and rearrangement. The lubrication effect of pore water reduces the frictional resistance between coral sand particles in relative motion, causing ϕ_u to decrease as S_r increases. Additionally, the lubrication action of pore water intensifies

the relative motion between coral sand particles, causing particle breakage quantity to rise with increasing Sr . The intensification of particle breakage weakens the shear strength of coral sand [40], and φ_b , affected by particle breakage, also decreases with increasing Sr . In addition, under the combined action of σ'_3 and particle breakage, coral sand samples in testing exhibited a small dilation degree or not at all (Figure 5), indicating that φ_d has a low weight in φ and exerts a small effect. Therefore, φ was mainly controlled by φ_u and φ_b , which both decreased as Sr dropped, resulting in a negative correlation between φ and Sr .

(2) Within the σ'_3 range of 800 kPa, coral sand samples with 90–100% Sr in UU triaxial shear stress state possessed a c . c fluctuated within a small range with changing Sr , but no apparent law of change was observed. c had a range of 280–310 kPa and was mainly concentrated between 300 and 310 kPa. The maximum difference in c between coral sand samples with various Sr levels was 25.3 kPa only (Figure 13b). According to classical soil mechanics, sandy soil has no cohesion. However, there is capillarity attraction in unsaturated sandy soil, and suitable water content produces an obvious cohesive action. The cohesion existing in these forms is also called “pseudo cohesion” or “apparent cohesion” [56]. The change in Sr affects the content and distribution of capillary water in coral sand, so Sr affects the apparent cohesion of coral sand. Meanwhile, in the τ – σ stress space, the UU shear strength envelope curves of coral sand samples with different Sr levels were almost parallel to the σ axis, so the c corresponding to the intercept of coral sand changed a little.

4. Particle Breakage Analysis

4.1. Effect of Saturation on Particle Breakage Ratio

The particle gradation curves of geomaterials change upon breakage. The particle breakage degree of a geomaterial can be quantified by the differences in its particle gradation curves before and after testing [57]. Hardin [58] mentioned that geomaterials with different initial gradations break into powder particles with sizes of less than 0.074 mm under sufficiently large external loads. On this basis, Hardin proposed a particle breakage evaluation indicator, i.e., relative breakage ratio (B_r):

$$B_r = \frac{B_t}{B_p} \quad (11)$$

where B_t denotes the total breakage, which is the area enclosed by the particle gradation curves before and after testing and the vertical line of $d = 0.074$ mm, and B_p denotes breakage potential, which is the area enclosed by the particle gradation curve before testing and the vertical line of $d = 0.074$ mm (Figure 14).

The B_r of coral sand under each condition was calculated using Equation (11) and the results of particle screening tests. Figure 15 shows the relationship between B_r and Sr for coral sand in the UU triaxial shear stress state. As can be seen from Figure 15, B_r increase with increasing Sr , which coincides with the research results of Wu et al. [9]. A coral sand sample with a higher Sr level has a higher pore water content, producing a lubrication action in interparticle relative motion. The lubrication action of pore water makes it easier for coral sand particles to experience rolling and displacement. In contrast, the increase in the probability of coral sand particles results in fracturing, abrading, or otherwise breaking them into relative motion, which causes a higher B_r .

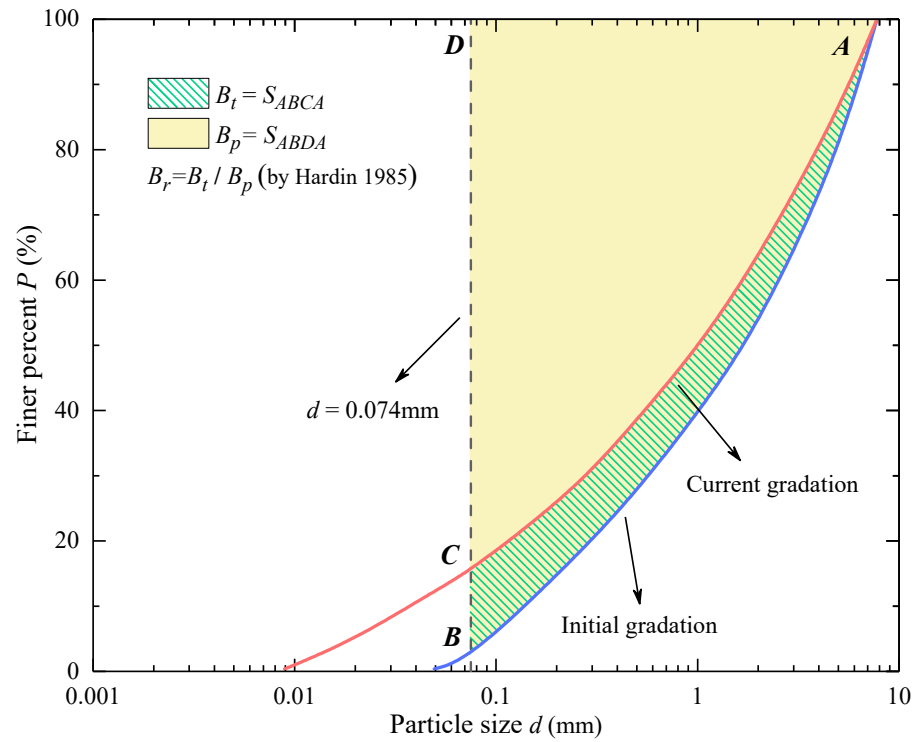


Figure 14. Calculated method of relative breakage ratio B_r .

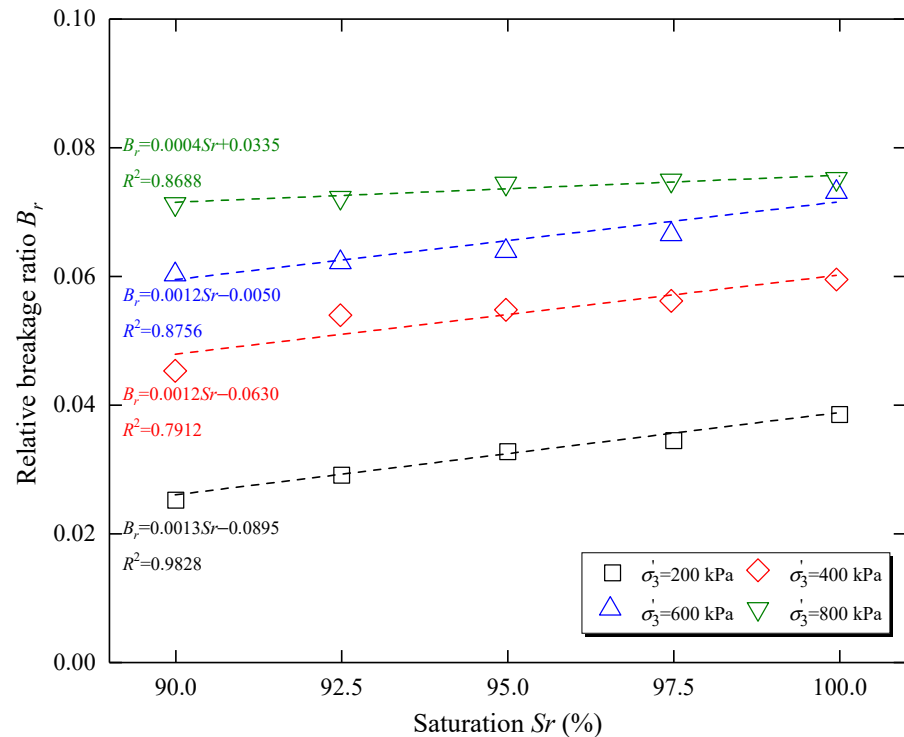


Figure 15. Relationship between relative breakage ratio and saturation of coral sand.

Further analysis revealed a good linear relationship between B_r and S_r for coral sand, which could be expressed as:

$$B_r = p_1 S_r + p_2 \tag{12}$$

where p_1 and p_2 are fitting parameters, p_1 is a positive value that characterizes the degree to which the B_r of coral sand increases with increasing S_r , and p_2 characterizes the combined

effect of other factors (such as compactness, stress level, and particle gradation) on the B_r of coral sand. The S_r effects on coral sand particle breakage disappeared when σ'_3 was sufficiently large. For example, when $\sigma'_3 = 200, 400,$ and 600 kPa, p_1 was 0.0012, 0.0012, and 0.0013, respectively, and the fitting curves were parallel to each other. When $\sigma'_3 = 800$ kPa, p_1 was 0.0004, and B_r increased very slightly with increasing S_r . When σ'_3 was sufficiently large, the intensification of particle breakage produced more fine particles that can be used to fill interparticle spacings. Thus, the presence of these fine particles obstructed the flow of pore water and further weakened its lubrication action on interparticle relative movement. This explains why S_r exerts little effect on the particle breakage of coral sand under a high value of σ'_3 . In addition, the production of fine particles caused particle breakage to stabilize by increasing σ'_3 gradually, which means that the particle breakage cannot proceed infinitely with increasing σ'_3 [59]. This phenomenon is pronounced at high S_r coral sand (Figure 15).

In the studies of coral sand particle breakage, saturated coral sand was the main target. In view of this, particle breakage results of coral sand with 100% S_r in this test are selected to compare with those introduced from other tests [18,25,27–29,33,60]. Figure 16 shows the particle breakage results of saturated coral sand under different conditions. It can be seen from Figure 16 that, B_r of coral sand is different due to the influence of sand origin, particle gradation, drained condition, compactness, and so on. Within the σ'_3 range of 800 kPa, B_r of coral sand is mainly distributed between 0.01 and 0.12, and B_r shows a significant positive correlation with σ'_3 . On the whole, B_r of coral sand in this test is relatively small, mainly for the following reasons: (I) The compactness of sand sample undergoes isotropic compression increases, and B_r increases accordingly. While sand sample in this test was not consolidated, resulting in a decrease of B_r . (II) Figure 16 illustrates that B_r of coral sand under drained condition is greater than under undrained condition, and this test was conducted under undrained condition, so B_r is relatively small. (III) Coral sand with finer particle size has less potential to breakage [17,18]. Coral sand used in this test was medium size, which is finer than sand in other tests, so B_r in the test is smaller.

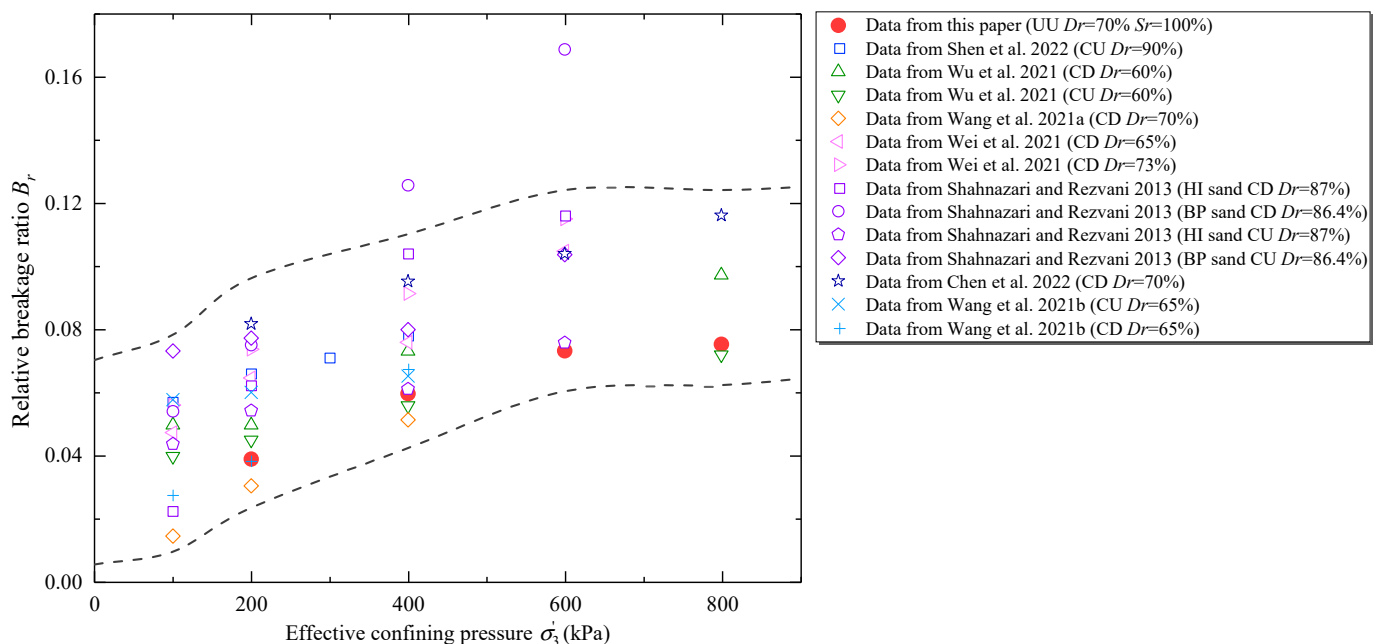


Figure 16. Previous test results of particle breakage of coral sand [25,27,28,33,39,60].

Furthermore, Wu et al. [9] measured the particle breakage of coral sand with different moisture contents based on CD triaxial shear test. Figure 17 shows the particle breakage results of Wu and this paper. The test result in this paper illustrated that there was a positive relationship between B_r and S_r for coral sand with $S_r \geq 90\%$. Test results in Wu's paper showed that there was also a positive relationship between B_r and S_r for coral sand

with S_r ranging from 17 to 69%. Further analysis indicates that Wu' data and the data in this paper can be described by the same linear expression with a great fit. In above, it can be inferred that there is a linear relationship between B_r and S_r of coral sand, and the relationship does not rely on S_r level of coral sand. However, the conditions of Wu' test are different from those in this paper (such as particle gradation, drained condition), and this speculation still needs to be verified by further experiments.

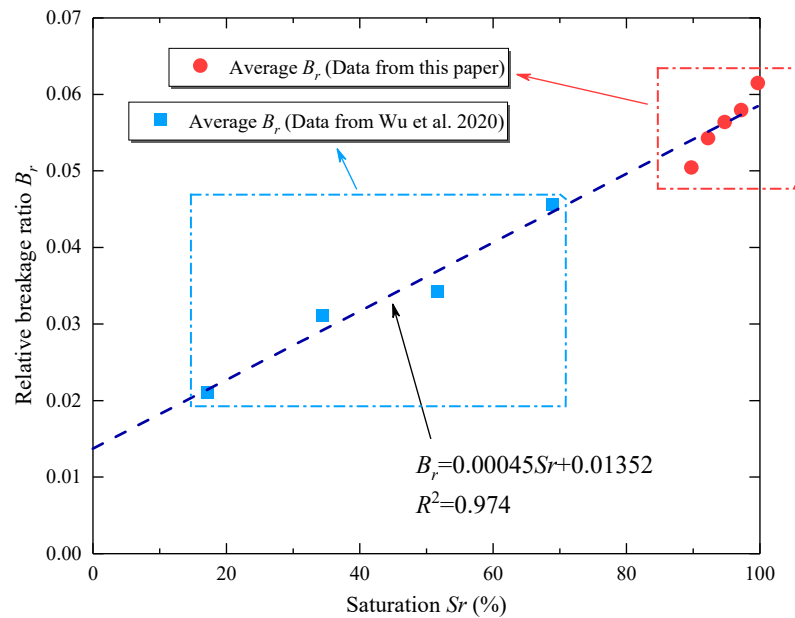


Figure 17. Relationship between relative breakage ratio and saturation combined with data from Wu et al. [9].

4.2. Effect of Saturation on Modified Particle Breakage Index

The calculation of B_r is based on the condition that the particle breakage limit is $d = 0.074$ mm. However, this condition is controversial. Subsequent studies showed that particles do not completely break into powder particles even when subjected to high stresses with values of about 689 MPa [61]. Einav [62] claimed that the limit of particle breakage obeys the following function:

$$f(d) = \left(\frac{d}{d_M}\right)^{3-\alpha} \tag{13}$$

where $f(d)$ denotes the ultimate particle gradation curve, d_M denotes the upper limit of particle size, and α denotes fractal dimension, set at 2.6 [63]. On this basis, Einav introduced the modified relative breakage index (B_r^*):

$$B_r^* = \frac{B_t}{B_p^*} \tag{14}$$

where B_t denotes total breakage, the value of which is the area enclosed by the initial particle gradation curve and the current particle gradation curve, and B_p^* denotes modified breakage potential, the value of which is the area enclosed by the initial particle gradation curve and the ultimate particle gradation curve (Figure 18).

The coral sand B_r^* under each condition was calculated according to Equation (14) and the results of particle screening tests. Figure 19 shows the relationship between B_r^* and S_r for coral sand in UU triaxial shear stress state. Under the same value of σ'_3 , the B_r^* of coral sand increased linearly with increasing S_r . When σ'_3 was sufficiently large, the growth rate of B_r^* with increasing S_r dropped significantly. As particle breakage evaluation indicators, B_r and B_r^* were similar in some aspects but different in others [29]. B_r and B_r^*

were similar in that they can describe the objective laws governing the particle breakage of coral sand in the same manner. B_r and B_r^* both depend on the initial particle gradation curve and the current particle gradation curve for calculating the actual particle breakage quantity. The initial particle gradation curve and the current particle gradation curve were definite values under given test conditions. They were different in that B_r^* was always greater than B_r under the same test conditions. A comparison between Equations (11) and (14) revealed that their main difference was the denominators. Due to the difference in ultimate gradation, B_p^* was always smaller than B_p under the same conditions, which was the main reason why B_r^* was greater.

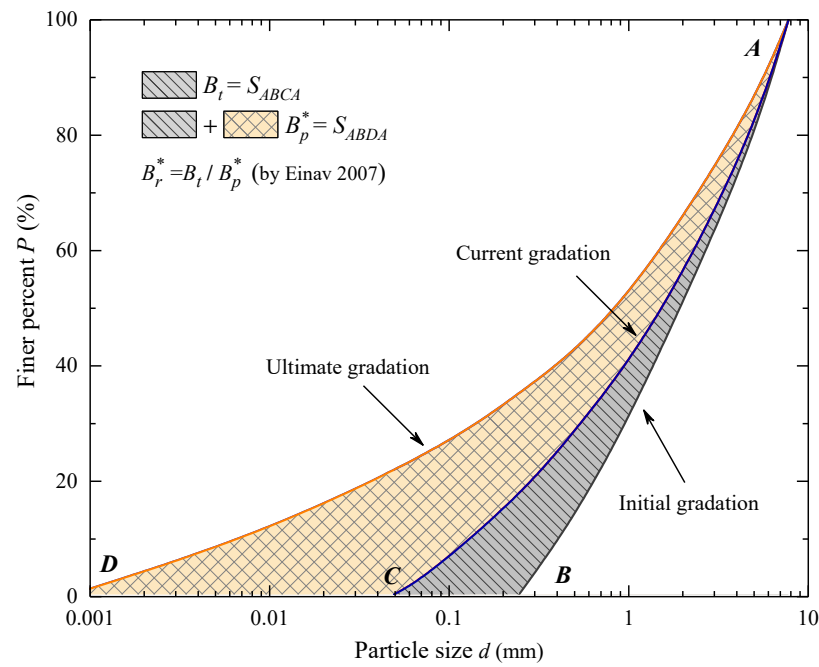


Figure 18. Calculated method of modified relative breakage index B_r^* .

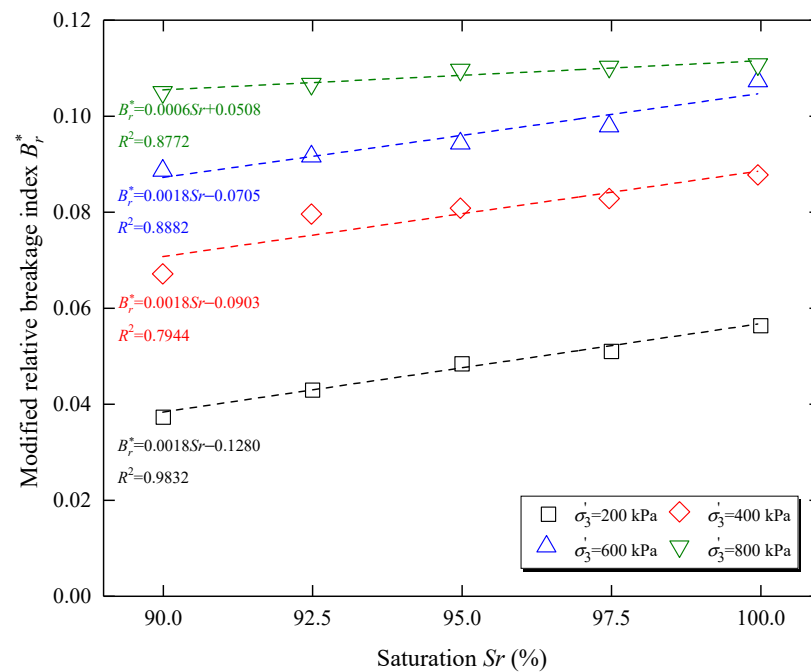


Figure 19. Relationship between modified relative breakage index and saturation of coral sand.

4.3. Effect of Saturation on Particle Median Size

Coral sand samples with different S_r levels experienced varying degrees of particle breakage in the shear process. Since some sand particles would break into finer sand particles, the median particle size (d_{50}) of samples would change accordingly. After testing, the d_{50} values of coral sand samples were calculated and then statistically investigated. Additionally, box plots were used to present the law of d_{50} changing with S_r . As seen from Figure 20, the mean and median d_{50} values of coral sand both decrease with increasing S_r . That is, under the same conditions, a sample with a higher S_r level can produce more fine particles after shear tests, suggesting that a higher S_r level means a larger particle breakage quantity for coral sand. This result is consistent with the result in Figure 15 (or Figure 19).

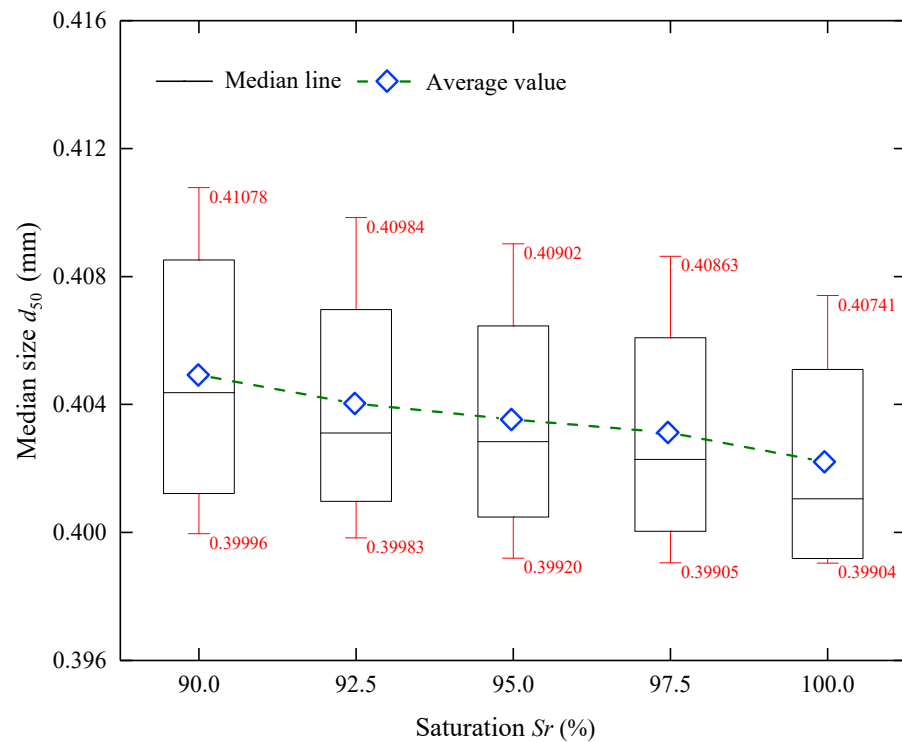


Figure 20. Relationship between median particles size and saturation of coral sand.

Figure 21 shows the relationships of d_{50} with B_r and B_r^* . It can be seen from Figure 21 that d_{50} decreases with increasing B_r and B_r^* , with linear fitting degrees of 0.9994 and 0.9989, respectively. A sample with a large particle breakage degree would produce more particles in the shear process, and consequently, the particle size corresponding to the cumulative percentage of particle size contents of 50% would be smaller. Thus, it can be observed that there is a negative correlation between d_{50} and particle breakage quantity.

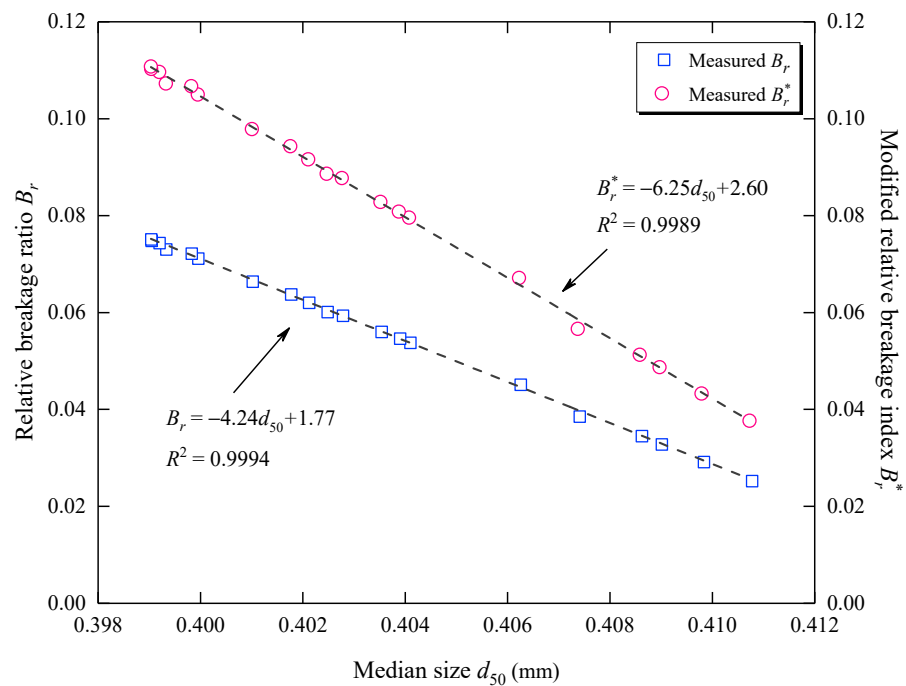


Figure 21. Relationship between relative breakage ratio, modified relative breakage index, and median particle size of coral sand.

5. Discussion of Saturation Effect on Shear Strength and Particle Breakage

5.1. Saturation Effect on Shear Strength of Coral Sand

The strength characteristics of coral sand samples with different *Sr* levels (90, 92.5, 95, 97.5, and 100%) are discussed. It was found that the strength characteristics of coral sand are basically consistent under 97.5% *Sr* and 100% *Sr* (Table 7). Therefore, 97.5% can be taken as the critical *Sr* of coral sand from the strength perspective. The mechanical properties of coral sand become stable after reaching the critical *Sr*, in that case, further increasing *Sr* produces no practical significance. In contrast, the *Sr* effect of the mechanical properties of coral sand is significantly below the critical *Sr*.

Table 7. Comparison in shear behavior between coral sand with 97.5% saturation and 100% saturation.

Shear Behavior	Saturation		
	<i>Sr</i> = 97.5%	<i>Sr</i> = 100%	
Shear strength <i>q_p</i> (kPa)	$\sigma'_3 = 200$ kPa	1240.1	1220.9
	$\sigma'_3 = 400$ kPa	1639.9	1638.1
	$\sigma'_3 = 600$ kPa	1813.2	1806.2
	$\sigma'_3 = 800$ kPa	2159.7	2147.1
Internal friction angle φ (°)	25.16	25.25	
cohesion <i>c</i> (kPa)	309.33	303.96	

In view of this, Equation (15) was used to calculate the ratio of the difference between the shear strength of coral sand below the critical *Sr* and that of coral sand at the critical *Sr* as follows:

$$\eta = \frac{(q_p)_i - (q_p)_{97.5}}{(q_p)_{97.5}} \times 100\% \tag{15}$$

where η denotes the ratio at which the shear strength of coral sand increases with decreasing *Sr*, and $(q_p)_i$ denotes the q_p of coral sand with a specific *Sr* (where *i* was set at 90, 92.5, and 95, respectively). Figure 22 shows the relationship between η and *Sr*. σ'_3 was taken as the threshold to calculate mean η and plot it in the figure. As seen in Figure 22, the η values for

coral sand with 90% S_r fall within the range of 10–20%. At this point, the shear strength of the sample, compared with that of coral sand with the critical S_r , is greatly improved, and can easily cause stress that exceeds the sensor range in the test process. Additionally, it can be seen that the η values of coral sand with 95% S_r are all less than 5%, suggesting that the shear strength of the sample with 95% S_r was extremely close to that with the critical S_r . The mean η value of coral sand with 92.5% S_r was 3.43% under a low effective confining pressure ($\sigma'_3 \leq 400$ kPa), and 8.14% under high effective confining pressures ($\sigma'_3 = 600$ and 800 kPa).

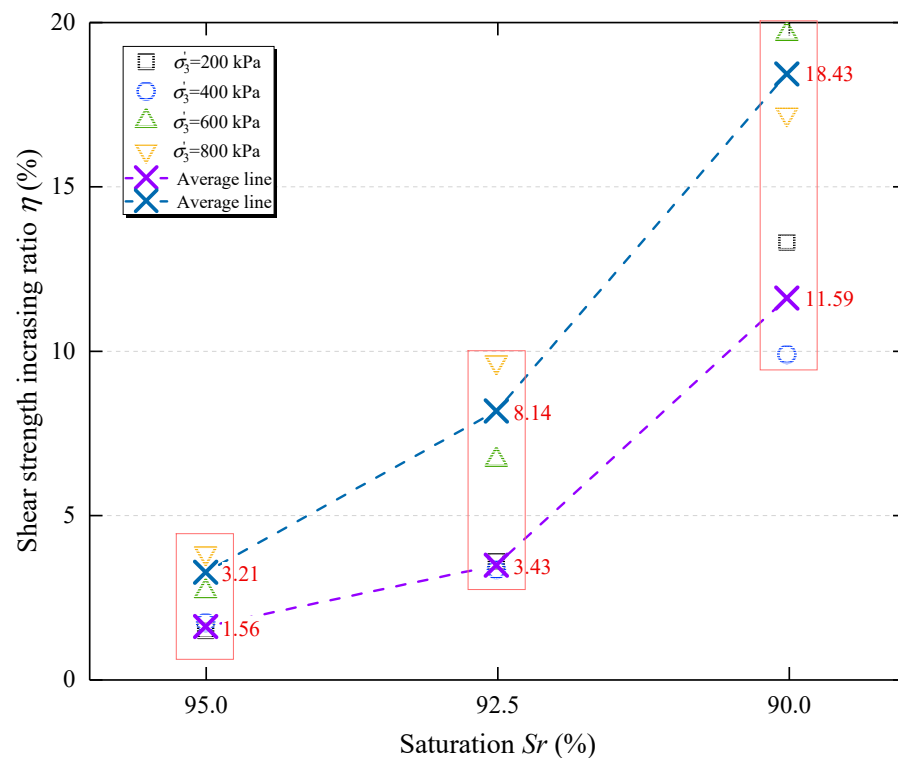


Figure 22. Relationship between shear strength increasing ratio and saturation of coral sand.

The preparation of saturated coral sand usually requires back pressure saturation to increase S_r , and $B > 0.95$ is often used as the criterion for the saturation of coral sand. To that end, it is often necessary to apply very high back pressure on coral sand [14,25,28,33,59,64]. However, coral sand is a special geomaterial that is susceptible to particle breakage even under normal stress. Accordingly, excessively high back pressure greatly modifies the original gradation of coral sand, causing changes in the mechanical properties of coral sand [65,66]. This study discusses the S_r effect on the strength of coral sand and aims to find a suitable S_r in an unsaturated region. It was found that the strength characteristics of coral sand with this S_r are roughly similar to those in the saturated state and that the applied back pressure on the sample at this point declines considerably (the B value was even smaller). On the basis of the above analysis, 92.5% S_r can be considered a suitable S_r value. Under this S_r , the strength of coral sand is close to that of saturated coral sand, and the B value corresponding to this S_r is 0.27, which is far less than the 0.95 required in the test code. Taking 92.5% as the S_r value of coral sand available for tests not only avoids the back pressure effect in the saturation process but also offers an idea for seeking a suitable saturation method for coral sand.

5.2. Saturation Effect on Particle Breakage of Coral Sand

Section 5.1 proposes a S_r value of coral sand available for tests. This section further demonstrates this conclusion from the perspective of particle breakage. Particle breakage is an irreversible physical process of particles splitting into fine particles, affecting geomateri-

als' strength, deformation characteristics, and energy absorption [67–70]. According to the calculation results in Section 4, when $\sigma'_3 = 200, 400, 600,$ and 800 kPa, the particle breakage quantities of coral sand with 92.5% S_r in the shear process are 0.00538, 0.00224, 0.00439, and 0.00268 less than that of the coral sand with the critical S_r , respectively. The particle breakage quantity of coral sand was smaller under a low S_r , in which case particle breakage exerted an even smaller effect on the strength characteristics of coral sand. Moreover, taking 92.5% as the S_r value of the coral sand available for tests in the preparation of coral sand can prevent particle breakage caused by the application of back pressure. The above discussion verifies the reasonableness of taking 92.5% as the S_r value of coral sand available for tests from the perspective of particle breakage.

6. Conclusions

To ascertain the saturation effect of the shear behavior of coral sand, this study conducted multiple groups of UU triaxial shear tests on coral sand samples with different S_r levels, and tested the particle breakage quantities of coral sand. The main conclusions of this study are as follows:

(1) Coral sand samples with different S_r levels all manifested strain softening characteristics. Increasing S_r promoted the development of u_{p1} in coral sand during the initial shear stage but had no effects on the E_i of coral sand.

(2) The shear strength of coral sand decreased exponentially with increasing S_r . The φ of coral sand decreased by 3.77° with the increase of S_r from 90% to 97.5%. However, when S_r increased from 97.5% to 100%, the φ of coral sand remained unchanged. The c of coral sand in this study fluctuated within the range of 280–310 kPa but was not considerably affected by S_r .

(3) For σ'_3 range of 600 kPa, the particle breakage quantity of coral sand increased linearly at a slope of 0.12% with increasing S_r . As the σ'_3 continued to rise, the linear increase rate of particle breakage quantity with increasing S_r declined to 0.04%. After testing, the d_{50} of coral sand decreased with increasing S_r or particle breakage quantity.

(4) 97.5% could be taken as the critical S_r of coral sand. Above this critical S_r , the mechanical properties of coral sand were stable. In contrast, below this critical S_r , the mechanical properties of coral sand were significantly affected by S_r . On the basis of comparing the strength and particle breakage characteristics of unsaturated coral sand and coral sand in a critical saturation state, this study suggested that 92.5% should be taken as the S_r value of coral sand available for tests.

Author Contributions: X.C.: Conceptualization, methodology, and writing—original draft; J.S.: investigation and project administration; X.W.: formal analysis and writing—original draft; T.Y.: writing—review and editing; D.X.: writing—review and editing. All authors have read and agreed to the published version of the manuscript.

Funding: This research was funded by the National Natural Science Foundation of China (Nos. 41772336, 42177151, and 42177154).

Data Availability Statement: Some or all data, models, or codes generated or used during this study are available from the corresponding author upon request.

Conflicts of Interest: The authors declare on conflict of interest.

Nomenclature

CS	Coral sand
S_r	Saturation (Unit: %)
σ'_3	Effective confining pressure (Unit: kPa)
UU	Unconsolidated–undrained
CD	Consolidated–drained
CU	Consolidated–undrained
d	Particle size (Unit: mm)
d_{50}	Diameter that corresponds to an 50% finer in the particle gradation curve (Unit: mm)
ρ_d	Dry density (Unit: g/cm ³)
e	Void ratio
P	Mass percentage of particles smaller than a certain size (Unit: %)
C_u	Nonuniformity coefficient
C_c	Curvature coefficient
G_s	Specific gravity
ρ_{dmin}	Minimum dry density (Unit: g/cm ³)
ρ_{dmax}	Maximum dry density (Unit: g/cm ³)
e_{min}	Minimum void ratio
e_{max}	Maximum void ratio
D_r	Relative density (Unit: %)
v	Shear rate (Unit: mm/min)
ε_a	Axial strain (Unit: %)
n	Porosity
V_W	Volume of water inside sample (Unit: mm ³)
V_V	Volume of pores inside sample (Unit: mm ³)
V	Sample volume (Unit: mm ³)
q	Deviator stress (Unit: kPa)
q_p	Peak deviator stress (Unit: kPa)
u	Pore water stress (Unit: kPa)
u_{p1}	Peak pore water stress (Unit: kPa)
σ'_1	Effective major principal stress (Unit: kPa)
p'	Mean effective principal stress (Unit: kPa)
E_i	Initial elastic modulus (Unit: kPa)
E'_i	Mean initial elastic modulus (Unit: kPa)
m_1, m_2, m_3	Fitting parameters
τ	Shear stress acting on the shear plane (Unit: kPa)
σ	Normal stress on the shear plane (Unit: kPa)
φ	Internal friction angle (Unit: °)
c	Cohesion (Unit: kPa)
φ_u	Sliding friction angle (Unit: °)
φ_d	Dilatancy friction angle (Unit: °)
φ_b	Friction angle caused by particle breakage and rearrangement (Unit: °)
B_r	Relative breakage ratio
B_t	Total breakage
B_p	Breakage potential
p_1, p_2	Fitting parameters
α	Fractal dimension
d_M	Upper limit of particle size (Unit: mm)
B_p^*	Modified breakage potential
B_r^*	Modified relative breakage index
η	Shear strength increasing ratio (Unit: %)
B	Pore water stress index

References

1. Wang, X.; Wu, Y.; Cui, J.; Zhu, C.Q.; Wang, X.Z. Shape characteristics of coral sand from the South China Sea. *J. Mar. Sci. Eng.* **2020**, *8*, 803. [\[CrossRef\]](#)
2. Javdanian, H.; Jafarian, Y. Dynamic shear stiffness and damping ratio of marine calcareous and siliceous sand. *Geo-Mar. Lett.* **2018**, *38*, 315–322. [\[CrossRef\]](#)
3. Xu, L.J.; Wang, X.Z.; Wang, R.; Zhu, C.Q.; Liu, X.P. Physical and mechanical properties of calcareous soils: A review. *Mar. Georesour. Geotechnol.* **2021**, *40*, 751–766. [\[CrossRef\]](#)
4. Wang, X.Z.; Ding, H.Z.; Meng, Q.S.; Wei, H.Z.; Wu, Y.; Zhang, Y. Engineering characteristics of coral reef and site assessment of hydraulic reclamation in the South China Sea. *Constr. Build. Mater.* **2021**, *300*, 124263. [\[CrossRef\]](#)
5. Chen, J.F.; Akosah, S.; Ma, C.; Gidigas, S.S.R. Large-scale triaxial tests of reinforced coral sand with different grain size distributions. *Mar. Georesour. Geotechnol.* **2022**. [\[CrossRef\]](#)
6. Shen, J.H.; Xu, D.S.; Liu, Z.W.; Wei, H.Z. Effect of particle characteristics stress on the mechanical properties of cement mortar with coral sand. *Constr. Build. Mater.* **2020**, *260*, 119836. [\[CrossRef\]](#)
7. Chen, X.; Xu, D.S.; Shen, J.H.; Wei, H.Z.; Wang, R. Effect of particle size and particle distribution pattern on dynamic behavior of cemented calcareous sand. *Mar. Georesour. Geotechnol.* **2022**. [\[CrossRef\]](#)
8. Shen, J.H.; Wang, X.; Liu, W.B.; Zhang, P.Y.; Zhu, C.Q.; Wang, X.Z. Experimental study on mesoscopic shear behavior of calcareous sand material with digital imaging approach. *Adv. Civil Eng.* **2020**, *2020*, 8881264. [\[CrossRef\]](#)
9. Wu, Y.; Wang, X.; Shen, J.H.; Cui, J.; Zhu, C.Q.; Wang, X.Z. Experiment study on the impact of water content on the strength parameters of coral gravelly sand. *J. Mar. Sci. Eng.* **2020**, *8*, 634. [\[CrossRef\]](#)
10. Bishop, A.W.; Henkel, D.J. *The Measurement of Soil Properties in the Triaxial Test*; Edward Arnold: New York, NY, USA, 1962.
11. Sharma, S.S.; Ismail, M.A. Monotonic and cyclic behavior of two calcareous soils of different origins. *J. Geotech. Geoenviron. Eng.* **2006**, *132*, 1581–1591. [\[CrossRef\]](#)
12. Hassanlourad, M.; Rasouli, M.R.; Salehzadeh, H. A comparison between the undrained shear behavior of carbonate and quartz sands. *Int. J. Civ. Eng.* **2014**, *12*, 338–350.
13. Wu, Y.; Cui, J.; Li, N.; Wang, X.; Wu, Y.H.; Guo, S.Y. Experimental study on mechanical behavior and particle breakage characteristics of hydraulic filled coral sand on a coral reef island in the South China Sea. *Rock Soil Mech.* **2020**, *41*, 3181–3191. [\[CrossRef\]](#)
14. Zhang, C.Y.; Chen, M.; Hu, M.J.; Wang, X.Z.; Tang, J.J. Effect of fine particles content on shear strength of calcareous sand. *Rock Soil Mech.* **2019**, *40*, 195–202.
15. Saeidaskari, J.; Alibolandi, M.; Azizkandi, A.S. Undrained monotonic and cyclic behavior of Qeshm calcareous sand. *Mar. Georesour. Geotechnol.* **2021**, *39*, 798–811. [\[CrossRef\]](#)
16. Liu, M.C.; Hu, S.F.; Dai, P.F. Investigation on shear behavior of calcareous sand in South China sea in undrained triaxial tests. *China J. Highw. Transp.* **2022**, *35*, 69–76. [\[CrossRef\]](#)
17. Wang, X.; Wang, X.Z.; Shen, J.H.; Zhu, C.Q. Particle size and confining-pressure effects of shear characteristics of coral sand: An experimental study. *Bull. Eng. Geol. Environ.* **2022**, *81*, 97. [\[CrossRef\]](#)
18. Chen, Y.Y.; Tang, Y.; Guan, Y.F.; Liu, R.M.; Han, X.; Zhao, X.Q. Study on the mechanical properties of coral sands with different particle gradations. *Mar. Georesour. Geotechnol.* **2022**. [\[CrossRef\]](#)
19. Lv, Y.R.; Liu, J.G.; Zuo, D.J. Moisture effects on the undrained dynamic behavior of calcareous sand at high strain rates. *Geotech. Test. J.* **2018**, *42*, 20170412. [\[CrossRef\]](#)
20. Shen, J.H.; Hu, M.J.; Wang, X.; Zhang, C.Y.; Xu, D.S. SWCC of calcareous silty sand under different fines contents and dry densities. *Front. Environ. Sci.* **2021**, *303*, 682907. [\[CrossRef\]](#)
21. Xu, D.S.; Su, Z.Q.; Lalit, B.; Qin, Y. A hybrid FBG-based load and vibration transducer with a 3D fused deposition modelling approach. *Meas. Sci. Technol.* **2022**, *33*, 065106. [\[CrossRef\]](#)
22. Qin, Y.; Wang, Q.K.; Xu, D.S.; Yan, J.M.; Zhang, S.S. A FBG based earth and water pressure transducer with 3D fused deposition modeling approach for soil mass. *J. Rock Mech. Geotech.* **2022**, *14*, 663–669. [\[CrossRef\]](#)
23. Ding, Z.; He, S.H.; Sun, Y.F.; Xia, T.D.; Zhang, Q.F. Comparative study on cyclic behavior of marine calcareous sand and terrigenous siliceous sand for transportation infrastructure applications. *Constr. Build. Mater.* **2021**, *283*, 122740. [\[CrossRef\]](#)
24. Zhang, J.M.; Zhang, L.; Jiang, G.S.; Wang, R. Research on particle crushing of calcareous sands under triaxial shear. *Rock Soil Mech.* **2008**, *29*, 2789–2793.
25. Shahnazari, H.; Rezvani, R. Effective parameters for the particle breakage of calcareous sand: An experimental study. *Eng. Geol.* **2013**, *159*, 91–105. [\[CrossRef\]](#)
26. Yu, F.W. Particle breakage in triaxial shear of a coral sand. *Soils Found.* **2018**, *58*, 866–880. [\[CrossRef\]](#)
27. Wang, G.; Wang, Z.N.; Ye, Q.G.; Zha, J.J. Particle breakage evolution of coral sand using triaxial compression tests. *J. Rock Mech. Geotech. Eng.* **2021**, *13*, 321–334. [\[CrossRef\]](#)
28. Wang, X.; Liu, J.Q.; Cui, J.; Wang, X.Z.; Shen, J.H.; Zhu, C.Q. Particle breakage characteristic of a founding filling material on island-reefs in the South China Sea. *Constr. Build. Mater.* **2021**, *306*, 124690. [\[CrossRef\]](#)
29. Shen, J.H.; Wang, X.; Shan, Y.; Cui, J.; Chen, X.; Wang, X.Z.; Zhu, C.Q. Particle breakage and shape analysis of calcareous sand under consolidated-undrained triaxial shear. *Bull. Eng. Geol. Environ.* **2022**, *81*, 232. [\[CrossRef\]](#)
30. Lv, Y.R.; Li, X.; Wang, Y. Particle breakage of calcareous sand at high strain rates. *Powder Technol.* **2020**, *366*, 776–787. [\[CrossRef\]](#)

31. Xu, L.J.; Wang, R.; Xu, D.S.; Wang, X.Z.; Meng, Q.S.; Zhu, C.Q. Review of particle breakage measurement methods for calcareous sand. *Adv. Civ. Eng.* **2022**, *2020*, 6477197. [[CrossRef](#)]
32. Wang, G.; Ye, Q.G.; Zha, J.J. Experimental study on mechanical behavior and particle crushing of coral sand-gravel fill. *Chin. J. Geotech. Eng.* **2018**, *40*, 802–810.
33. Wu, Y.; Li, N.; Wang, X.Z.; Cui, J.; Chen, Y.L.; Wu, Y.H.; Yamamoto, H. Experimental investigation on mechanical behavior and particle crushing of calcareous sand retrieved from South China Sea. *Eng. Geol.* **2021**, *280*, 105932. [[CrossRef](#)]
34. Wang, C.Y.; Ding, X.M.; Yin, Z.Y.; Peng, Y.; Chen, Z.X. Mechanical characteristic and particle breakage of coral sand under one-dimensional repeated loading. *Acta Geotech.* **2021**, *17*, 3117–3130. [[CrossRef](#)]
35. Maleki, M.; Bayat, M. Experimental evaluation of mechanical behavior of unsaturated silty sand under constant water content condition. *Eng. Geol.* **2012**, *141*, 45–56. [[CrossRef](#)]
36. Duong, T.V.; Tang, A.M.; Cui, Y.J.; Trinh, V.N.; Dupla, J.C.; Calon, N.; Canou, J.; Robinet, A. Effects of fines and water contents on the mechanical behavior of interlayer soil in ancient railway sub-structure. *Soils Found.* **2013**, *53*, 868–878. [[CrossRef](#)]
37. Aldaood, A. Impact of fine materials on the saturated and unsaturated behavior of silty sand soil. *Ain Shams Eng. J.* **2020**, *11*, 717–725. [[CrossRef](#)]
38. Wang, X.; Wu, Y.X.; Lu, Y.; Cui, J.; Wang, X.Z.; Zhu, C.Q. Strength and dilatancy of coral sand in the South China Sea. *Bull. Eng. Geol. Environ.* **2021**, *80*, 8279–8299. [[CrossRef](#)]
39. Shen, J.H.; Wang, X.; Cui, J.; Wang, X.Z.; Zhu, C.Q. Shear characteristic of calcareous gravelly sand considering particle breakage. *Bull. Eng. Geol. Environ.* **2022**, *81*, 130. [[CrossRef](#)]
40. Zhang, J.M.; Jiang, G.S.; Wang, R. Research on influences of particles breakage and dilatancy on shear strength of calcareous sand. *Rock Soil Mech.* **2009**, *30*, 2043–2048.
41. Hassanlourand, M.; Salehzadeh, H.; Shahnazari, H. Dilation and particle breakage effects on the shear strength of calcareous sand based on energy aspects. *Int. J. Civ. Eng.* **2008**, *6*, 108–119.
42. Wang, X.Z.; Jiao, Y.Y.; Wang, R.; Hu, M.J.; Meng, Q.S.; Tan, F.Y. Engineering characteristics of calcareous sand in Nansha Islands, South China Sea. *Eng. Geol.* **2011**, *120*, 40–47. [[CrossRef](#)]
43. Khaboushan, E.A.; Emami, H.; Mosaddeghi, M.R.; Astarai, A.R. Estimation of unsaturated shear strength parameters using easily-available soil properties. *Soil Trill Res.* **2018**, *184*, 118–127. [[CrossRef](#)]
44. Wei, Y.J.; Wu, X.L.; Xia, J.W.; Miller, G.A.; Cai, C.F.; Guo, Z.L.; Hassanikhah, A. The effect of water content on the shear strength characteristics of granitic soils in South China. *Soil Trill Res.* **2019**, *187*, 50–59. [[CrossRef](#)]
45. Shen, J.H.; Wang, X.Z.; Wang, X.; Yao, T.; Wei, H.Z.; Zhu, C.Q. Effect and mechanism of fines content on the shear strength of calcareous sand. *Bull. Eng. Geol. Environ.* **2021**, *80*, 7899–7919. [[CrossRef](#)]
46. Xu, D.S.; Huang, M.; Zhou, Y. One-dimension compression behavior of calcareous sand and marine clay mixtures. *Int. J. Geomech.* **2020**, *20*, 04020137. [[CrossRef](#)]
47. Qin, Y.; Wang, Q.K.; Xu, D.S.; Fan, X.C. Study of the effects of fine coral powder and salinity on the mechanical behaviour of coral sand-seawater cement mortar. *Constr. Build. Mater.* **2021**, *313*, 125476. [[CrossRef](#)]
48. Yang, J.J.; Xu, D.S.; Shen, J.H.; Wei, H.Z.; Wang, R.; Xiao, X.B. Effect of coral sand powders and seawater salinity on the impact mechanical properties of cemented coral sand. *Soils Found.* **2022**, *62*, 101206. [[CrossRef](#)]
49. Wiebe, B.; Graham, J.; Tang, G.X.; Dixon, D. Influence of pressure, saturation, and temperature on the behaviour of unsaturated sand-bentonite. *Can. Geotech. J.* **1998**, *35*, 194–205. [[CrossRef](#)]
50. Hu, X.; Hong, B.N.; Du, Q.; Meng, Y.M. Influence of water contents on shear strength of coal-bearing soil. *Rock Soil Mech.* **2009**, *30*, 2291–2294.
51. Malizia, J.P.; Shakoar, A. Effect of water content and density on shear strength and deformation behavior of clay soils. *Eng. Geol.* **2018**, *244*, 125–131. [[CrossRef](#)]
52. Wang, X.Z.; Wang, X.; Jin, Z.C.; Meng, Q.S.; Zhu, C.Q.; Wang, R. Shear characteristics of calcareous gravelly soil. *Bull. Eng. Geol. Environ.* **2017**, *76*, 561–573. [[CrossRef](#)]
53. Alonso, E.E.; Pereira, J.M.; Vaunat, J.; Olivella, S. A microstructurally based effective stress for unsaturated soils. *Géotechnique* **2010**, *60*, 913–925. [[CrossRef](#)]
54. Rowe, P.W.; Barden, L.; Lee, I.K. Energy components during the triaxial cell and direct shear tests. *Géotechnique* **1964**, *14*, 247–261. [[CrossRef](#)]
55. Lee, K.L.; Farhoomand, I. Compressibility and crushing of granular soil in anisotropic triaxial tests. *Can. Geotech. J.* **2011**, *4*, 68–86. [[CrossRef](#)]
56. Wang, X.Z.; Weng, Y.L.; Wang, X.; Chen, J.W. Interlocking mechanism of calcareous soil. *Rock Soil Mech.* **2008**, *39*, 3113–3120. [[CrossRef](#)]
57. Lade, P.V.; Yamamuro, J.A.; Bopp, P.A. Significance of particle crushing in granular materials. *J. Geotech. Eng.* **1996**, *122*, 309–316. [[CrossRef](#)]
58. Hardin, B.O. Crushing of soils particles. *J. Geotech. Eng.* **1985**, *111*, 1177–1192. [[CrossRef](#)]
59. Yan, C.P.; Long, Z.L.; Zhou, Y.C.; Kuang, D.M.; Chen, J.M. Investigation on the effects of confining pressure and particle size of shear characteristics of calcareous sand. *Rock Soil Mech.* **2020**, *41*, 581–591.
60. Wei, H.Z.; Li, X.X.; Zhang, S.D.; Zhao, T.; Yin, M.; Meng, Q.S. Influence of particle breakage on drained shear strength of calcareous sands. *Int. J. Geomech.* **2021**, *21*, 04021118. [[CrossRef](#)]

61. Biarez, J.; Hicher, P.-Y. *Elementary Mechanics of Soil Behavior*; A.A.Balkema: Avereest, The Netherlands, 1994.
62. Einav, I. Breakage mechanics—Part I: Theory. *J. Mech. Phys. Solids* **2007**, *55*, 1274–1297. [[CrossRef](#)]
63. Cooper, M.R.; Sorensen, K.K.; Bodas Freitas, T.; Georgoutsos, G. Particle breakage during shearing of a carbonate sand. *Géotechnique* **2004**, *54*, 157–163. [[CrossRef](#)]
64. Gao, R.; Ye, J.H. Experimental investigation on the dynamic characteristics of calcareous sand from the reclaimed coral reef islands in the South China Sea. *Rock Soil Meth.* **2019**, *40*, 3897–3908.
65. Brand, E.W. Back pressure effects on the undrained strength characteristic of soft clay. *Soils Found.* **1975**, *15*, 1–16. [[CrossRef](#)]
66. Huang, B.; Wang, Q.J.; Ling, D.S.; Ding, H.; Chen, Y.M. Effect of back pressure on shear strength of saturated sand in triaxial tests. *Rock Soil Mech.* **2012**, *34*, 1313–1319.
67. Bandini, B.; Cooper, M.R. The influence of particle breakage on the location of the critical state line of sand. *Soils Found.* **2011**, *51*, 591–600. [[CrossRef](#)]
68. Yao, T.; Baudet, B.A.; Lourenco, S.D. Evolution of surface roughness of single sand grains with normal loading. *Géotechnique* **2022**, *72*, 543–555. [[CrossRef](#)]
69. Ovalle, C.; Dano, C.; Hicher, P.-Y.; Cisternas, M. Experimental framework for evaluating the mechanical behavior of dry and wet crushable granular materials based on the particle breakage ratio. *Can. Geotech. J.* **2015**, *52*, 587–598. [[CrossRef](#)]
70. Wei, H.Z.; Yin, M.; Zhao, T.; Yan, K.; Shen, J.H.; Meng, Q.S.; Wang, X.Z.; He, J.Q. Effect of particle breakage on the shear strength of calcareous sand. *Mar. Geophys. Res.* **2021**, *42*, 23. [[CrossRef](#)]